



# Enriched lithospheric mantle keel below the Scottish margin of the North Atlantic Craton: Evidence from the Palaeoproterozoic Scourie Dyke Swarm and mantle xenoliths



Hannah S.R. Hughes <sup>a,\*</sup>, Iain McDonald <sup>a</sup>, Kathryn M. Goodenough <sup>b</sup>, T. Jake R. Ciborowski <sup>a</sup>, Andrew C. Kerr <sup>a</sup>, Joshua H.F.L. Davies <sup>c</sup>, David Selby <sup>d</sup>

<sup>a</sup> School of Earth and Ocean Sciences, Cardiff University, Park Place, Cardiff CF10 3AT, UK

<sup>b</sup> British Geological Survey, West Mains Road, Edinburgh EH9 3LA, UK

<sup>c</sup> Department of Earth and Atmospheric Sciences, University of Alberta, Edmonton, Alberta T6G 2E3, Canada

<sup>d</sup> Department of Earth Sciences, Durham University, Durham DH1 3LE, UK

## ARTICLE INFO

### Article history:

Received 26 November 2013

Received in revised form 9 May 2014

Accepted 13 May 2014

Available online 9 June 2014

### Keywords:

Scourie Dyke

Lewisian

Lithospheric mantle

Mantle xenoliths

Metasomatism

PGE

## ABSTRACT

The Lewisian Gneiss Complex of NW Scotland represents the eastern margin of the North Atlantic Craton. It comprises mid-late Archaean tonalite-trondhjemite-granodiorite gneisses that were metamorphosed and deformed during the Late-Archaean and Palaeoproterozoic. A major swarm of mafic-ultramafic dykes, the Scourie Dyke Swarm, was intruded at ca. 2.4–2.3 Ga during a period of extension that can be correlated across the North Atlantic Craton. The majority of dykes are doleritic, with volumetrically minor picritic and olivine gabbro suites.

New major and trace element geochemical data and Re-Os isotopes indicate that the Scourie Dyke Swarm was not solely derived from a 'typical' asthenospheric mantle source region. The geochemical signatures of the dykes show significant negative Nb, Ta and Ti anomalies, coupled with enrichment in Th, Light Rare Earth Elements and other large ion lithophile elements. These features cannot be reproduced by simple contamination of asthenospheric sources with Lewisian granulite-facies crust. Instead they are a feature of the mantle source that produced the Scourie Dykes and may have developed during Archaean subduction episodes.

Spinel lherzolite mantle xenoliths from the Isle of Lewis offer direct insight into the lithospheric mantle below this region. They display similar geochemical 'enrichments' and 'depletions' observed in the Scourie Dykes and the magma source is thus considered to reside primarily in the sub-continental lithospheric mantle (SCLM), with some potential contribution from asthenospheric melts. Platinum Group Element geochemistry and trace element modelling indicate that the dolerite dykes were formed by moderate (<15%) partial melting of the source, whilst higher degrees of partial melting led to the formation of picritic and olivine gabbro suites. Magma production was triggered by significant crustal and lithospheric extension, causing both asthenospheric and substantial lithospheric melting.

© 2014 The Authors. Published by Elsevier B.V. This is an open access article under the CC BY license (<http://creativecommons.org/licenses/by/3.0/>).

## 1. Introduction

The Lewisian Gneiss Complex crops out in NW Scotland and the Outer Hebridean Islands. It comprises mid-late Archaean

tonalite-trondhjemite-granodiorite (TTG) gneisses, with minor mafic-ultramafic and metasedimentary components, that have been reworked by several Late Archaean and Palaeoproterozoic tectonic events. The Complex contains an extensive swarm of early Palaeoproterozoic mafic to ultramafic dykes (the Scourie Dykes) which can be correlated with dykes across the wider North Atlantic Craton (Bridgwater et al., 1995). The Scourie Dykes were first mapped by Peach et al. (1907) and were recognised as an important time marker by Sutton and Watson (1951). Distinctions were made between the dykes according to their relict igneous mineralogy and bulk geochemical properties (Weaver and Tarney, 1981b; Tarney and Weaver, 1987). Initial dating suggested that the dykes were intruded in two episodes, at ca. 2.4 and 2.0 Ga (Heaman

**Abbreviations:** SCLM, subcontinental lithospheric mantle; TTG, tonalite trondhjemite granodiorite; PGE, platinum group elements; IPGE, Ir-group PGE; PPGE, Pd-group PGE; LILE, large ion lithophile elements; LREE, light rare earth elements; MREE, middle rare earth elements; HREE, heavy rare earth elements; HFSE, high field strength elements; NAC, North Atlantic Craton; MSS, Monosulphide solid solution.

\* Corresponding author. Tel.: +44 029 208 74830.

E-mail addresses: [hughesH6@cf.ac.uk](mailto:hughesH6@cf.ac.uk), [hhughes2000@gmail.com](mailto:hhughes2000@gmail.com) (H.S.R. Hughes).

and Tarney, 1989) but only one dyke recorded the younger age. The majority of the dykes are now considered to have been emplaced in one magmatic event at ca. 2.418–2.375 Ga (Davies and Heaman, 2014).

The Lewisian Gneiss Complex is divided into a number of regions or terranes separated by major shear zones (Kiny et al., 2005; Fig. 1) with Scourie Dykes present in all terranes. Substantial work has focused on the Assynt Terrane, which comprises Archaean granulite-facies TTG gneisses locally reworked by post-Scourie Dyke amphibolite-facies metamorphism and deformation. To the north and south respectively, the Rhiconich and Gruinard Terranes were more thoroughly reworked at amphibolite-facies. Thus, igneous textures and mineralogy of the Scourie Dykes are best preserved in the Assynt Terrane (Tarney and Weaver, 1987). Scourie and 'Scourie-like' dykes have also been studied from the Rhiconich (Northern) Lewisian Terrane, the Isles of Coll and Tiree, and the Outer Hebrides (Fettes and Mendum, 1987; Muir et al., 1993; Mason and Brewer, 2004; Goodenough et al., 2010). In total this data set comprises ~50 Scourie Dyke analyses, spanning almost 30 years of varying analytical methods and differing element suites, for dykes found across the entire Lewisian Gneiss Complex.

In this paper, we present an updated data set of whole-rock geochemical analyses, including the platinum group elements (PGE), for the Scourie Dykes based on new sampling carried out across the three mainland Lewisian Terranes (Rhiconich, Assynt and Gruinard) using modern and consistent analytical techniques. These new data are used to re-assess the potential magma sources and provide insights into the geochemistry of Archaean subcontinental lithospheric mantle (SCLM) and melting regimes. In addition, we present whole-rock geochemical analyses and PGE concentrations of upper mantle (lithospheric) spinel lherzolite xenoliths from the Isle of Lewis, to directly investigate the geochemistry of the SCLM that underlies the Lewisian Gneiss Complex.

## 2. Regional geology

The Lewisian Gneiss Complex is a small fragment of the much larger North Atlantic Craton (NAC; Fig. 1c) that includes Greenland, Labrador and parts of Canada and which consists of Archaean protoliths with zones of Palaeoproterozoic reworking. Tectonic events within the Lewisian fragment were as follows: (1) 3.0–2.8 Ga – magmatic protolith formation, (2) 2.8–2.5 Ga high-grade metamorphism and deformation including initiation of shear zones, (3) 2.4–2.0 Ga – intrusion of mafic and ultramafic dyke swarms (the Scourie Dykes), (4) 2.0–1.8 Ga – formation and accretion of arc terranes, marked by calc-alkaline granitoid emplacement and related volcanics, and formation of localised high-grade Laxfordian metamorphic belts in the Lewisian portion of the NAC, (5) 1.8–1.5 Ga – continued calc-alkaline igneous activity, amphibolite-facies metamorphism and deformation, and crustal anatexis during the Laxfordian event (Park, 1994, 1995; Kiny et al., 2005; Goodenough et al., 2013; Vernon et al., 2014).

The mainland Lewisian Gneiss Complex has traditionally been sub-divided into three districts (Peach et al., 1907; Sutton and Watson, 1951): the Central granulite-facies district, which was only partially affected by Laxfordian-age reworking, and the North and South amphibolite-facies districts that were extensively reworked in the Laxfordian (Fig. 1a). Recent geochronological data have shown that these crustal blocks also have different protolith ages, and they are now considered to represent separate terranes divided by major shear zones (Friend and Kiny, 2001; Love et al., 2003; Kiny et al., 2005; Park et al., 2005; Goodenough et al., 2010; Love et al., 2010). The number of terranes or 'blocks' and the details of this model are still contentious, and timing and composition of the

Scourie Dykes are important (Goodenough et al., 2010). The terrane nomenclature of Kiny et al. (2005) has been adopted here (Fig. 1) with the Rhiconich, Assynt and Gruinard Terranes being broadly comparable to the North, Central, and South districts, respectively.

The Assynt and Rhiconich Terranes are separated by the Laxford Shear Zone, inferred to be a boundary between two crustal blocks (Goodenough et al., 2010). The Assynt Terrane consists of banded felsic gneisses of classic TTG composition, with mafic-ultramafic pods and lenses on scales from 1 cm to 10 m across. The typical granulite-facies gneisses are coarse-grained rocks containing clinopyroxene, hornblende, plagioclase and occasionally retrograde biotite (Johnstone and Mykura, 1989). However, unretrogressed granulite-facies lithologies are relatively rare; the majority of the Assynt gneisses display some degree of amphibolite-facies reworking, typically in discrete Laxfordian shear zones (Kiny et al., 2005). The Assynt gneisses are characterised by a marked depletion in U, Th, and the LILE (Sheraton et al., 1973).

The amphibolite-facies Rhiconich Terrane consists of more homogeneous biotite-hornblende gneisses of granodioritic composition (Goodenough et al., 2010). Lenses, sheets, and veins of Laxfordian pegmatite and granite are also present. In comparison with the Assynt Terrane, the Rhiconich amphibolite gneisses are richer in U, Th and the LILE (Frick et al., 1994; Holland and Lambert, 1973; Sheraton et al., 1973).

The Gruinard Terrane comprises hornblende-biotite-feldspar-quartz gneisses (amphibolite-facies) with a variety of mafic to ultramafic bodies on a range of scales (Fowler, 1986; Rollinson and Fowler, 1987). Geochemically, the Gruinard Terrane gneisses are more similar to those of the Rhiconich Terrane than the Assynt Terrane, and lack the strong U, Th and LILE depletion found in the latter.

### 2.1. Geology of the Scourie Dyke Swarm and previous work

The approximately NW-SE trend of the Scourie Dyke Swarm is thought to have been controlled by pre-existing shear zones that were exploited during crustal extension (Tarney, 1973). Many of the Scourie Dykes have been deformed and metamorphosed by Laxfordian shearing, but their igneous mineralogy and textures are still preserved at some localities in the Assynt Terrane. Similar dykes (the 'Older Basics') have also been described from the Outer Hebrides (Fettes and Mendum, 1987) but were not sampled during this study. The Scourie Dyke Swarm forms part of a wider Palaeoproterozoic group of basic dyke swarms extending throughout Labrador, Western and Eastern Greenland, and Baltica. These include the Kangâmiut, Graedefjord and Avayalik mafic dykes in W Greenland (Kalsbeek et al., 1987; Bridgwater et al., 1995; van Gool et al., 2002; Nilsson et al., 2013); high-Mg dyke swarms in Karelia and Kola (Fennoscandia); and Eqluk, Kangeq, and Aornit high-Mg dykes in SW Greenland (Bridgwater et al., 1995, and references therein).

In the Assynt Terrane, two generations of Scourie dykes are apparent: a mafic suite trending NW-SE, and an ultramafic E-W trending suite (Weaver and Tarney, 1981b; Tarney and Weaver, 1987). Both suites are steep-sided, ranging in width from 30 to 100 m, and some dykes can be traced along strike for up to 15 km, often with tapering offshoots (Weaver and Tarney, 1981b). They display sharp contacts with the host gneisses, and cross-cut pre-existing structures.

Petrological and geochemical features of the Scourie Dyke Swarm in the Assynt Terrane were reported by Tarney (1963, 1973), Weaver and Tarney (1981b), and Tarney and Weaver (1987) who grouped the dykes according to their original igneous mineralogy and composition. Four suites of dyke were identified: a main 'quartz-dolerite' or 'dolerite' suite (comprising 90–95% of all dykes

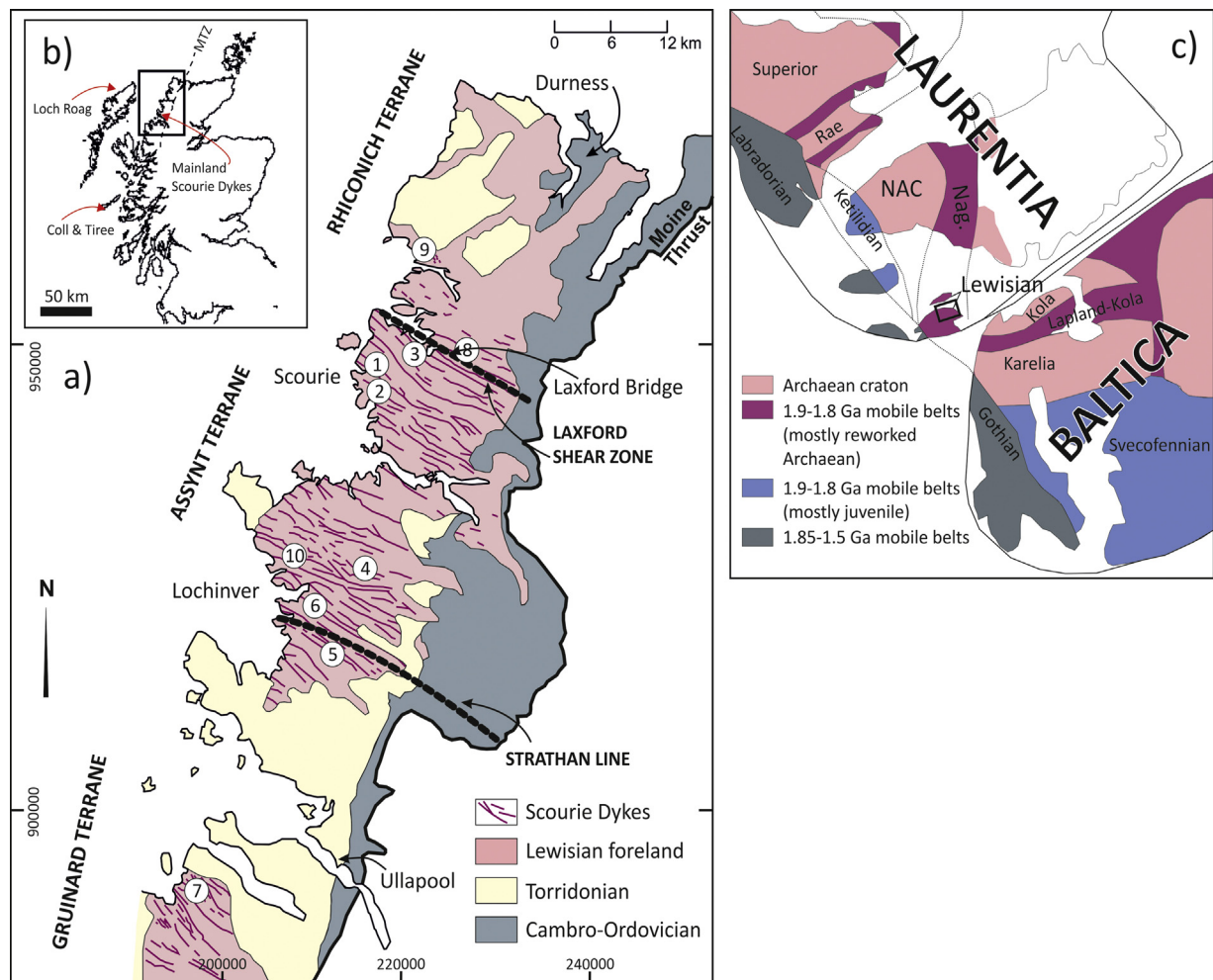


**Fig. 1.** (a) Simplified map of NW Scotland, showing main geological units and the Scourie Dykes and location of Loch Roag mantle xenolith site (b). MTZ is Moine Thrust Zone, delineating the Caledonian Foreland. Numbered localities indicate approximate dyke sampling locations. Terrane nomenclature based on Kinniy et al. (2005). (c) Larger scale simplified map showing the early Palaeoproterozoic relationship between the Lewisian of Scotland and the North Altantic Craton, as part of Laurentia and Baltica, based on Buchan et al. (2000).

in the Assynt Terrane), and comparatively minor ‘bronzite-picrites’ (here referred to as ‘picrites’), ‘olivine-gabbro’, and rare ‘norite’ suites which were not collected during this study (Tarney, 1973; Weaver and Tarney, 1981b; Tarney and Weaver, 1987). Field evidence suggests that the main dolerite suite was the first dyke group to be intruded, with subsequent picrite and olivine gabbro dykes cross-cutting them (Tarney, 1973). Due to limited exposure, and the general scarcity of ultramafic relative to mafic dykes, there are only a few places where this relationship can be observed. Recent geochronological work on the Scourie Dyke Swarm reveals that the main pulse of dolerite dyke intrusion occurred between 2.418 and 2.375 Ga (Davies and Heaman, 2014). However subtleties of the timing within this event have also been identified. For example some of the ultramafic dykes are in fact older than the mafic dykes (Davies and Heaman, 2014) so that within this ‘main’ event the Scourie Dykes were intruded in the following order; (1) an older minor suite (2418–2408 Ma) of ultramafic dykes, (2) the major suite of mostly mafic dykes with some ultramafics (2395–2390 Ma), and (3) a late suite of mafic dykes (2385–2375 Ma). The very late event at ~2000 Ma, identified by Heaman and Tarney (1989) has not been recognised again in recent studies, suggesting that it was a comparatively minor component of magmatism.

The dyke grouping criteria, maps and sampling locations for the Assynt Terrane from Weaver and Tarney (1981b), Tarney and Weaver (1987) were used during this study, in an attempt to ensure

that all dyke suites were characterised. Dykes were also sampled from the Rhiconich and Gruinard Terranes. Geochemically, these are all basaltic dykes, rather than picrite or olivine gabbro.

The mineralogy and petrology of the three analysed dyke suites are as follows (Weaver and Tarney, 1981b; Tarney and Weaver, 1987):

- (1) Dolerite dykes – These are texturally and mineralogically uniform with chilled margins. Almost complete amphibolitisation is common, with acicular networks of tremolite–actinolite (or ‘uralisation’). Reliable estimates of primary mineral modal abundances are difficult, but overall they consist of (partially) amphibolitised clinopyroxene, (partially) amphibolitised minor orthopyroxene, plagioclase, hornblende, quartz, and biotite. Accessory magnetite, ilmenite, pyrite, pyrrhotite and apatite are present.
- (2) Picrite dykes comprise up to 55% olivine, 5–80% orthopyroxene, 7–30% clinopyroxene, interstitial plagioclase (7–25%), minor phlogopite (1–4%), accessory chromite, Fe-Ti oxides and pyrite. Each dyke has a distinctive texture and olivine size range (uniform per dyke) and plagioclase is interstitial to pyroxenes. No chilled margins are observed in these dykes, which instead have coarse pyroxene-rich margins.
- (3) Olivine gabbro dykes are composed of 3–6% orthopyroxene, 20–38% clinopyroxene, 12–20% olivine, 20–35% plagioclase,

8–16% hornblende and minor phlogopite (3–8%). Accessory magnetite, ilmenite, pyrite and pyrrhotite are present, and spherulitic clinopyroxene is generally concentrated at dyke margins.

Primary hydrous phases such as hornblende, phlogopite or biotite indicate a deep intrusion level of dykes (O'Hara, 1961; Tarney, 1963, 1973), where magmatic volatile components were retained, and could be suggestive of a hydrated magma source. Where undeformed, dyke chilled margins are composed of hornblende, plagioclase, and sometimes garnet, implying a high ambient temperature of the crust during emplacement (300–500 °C). This could also suggest a deep level of intrusion (O'Hara, 1961; Tarney, 1973) and is consistent with the mineralogy and the coarse-grained gabbroic textures observed at dyke centres. Dyke margins are sharp and well defined with rare examples of marginal xenoliths (e.g., at Upper Badcall, dyke samples X40, 41 and 42) but little other observable evidence of contamination.

Laxfordian amphibolite-facies metamorphism of the dykes is common as shown by variable amounts of 'amphibolisation' to tremolite and actinolite (Tarney, 1963). Garnet occurs in some Assynt Terrane dolerite dykes, sometimes as coarse stringers (e.g., 'the Graveyard dyke', Scourie Bay). Garnet is also prevalent in dykes around Gairloch (Gruinard Terrane) as patches or lenses. These dykes have compositions distinct from other members of the Scourie Dyke Swarm (Park, 2002 – Shieldaig dykes) and this may have facilitated the growth of garnet during metamorphism. Although primary igneous mineralogy is retained to some degree at localities in the Assynt Terrane, an amphibolite-facies overprint is often present. This is particularly the case for earlier mafic dykes, with primary mafic silicates almost entirely replaced by hornblende. Amphibolitisation increases from the dyke centres to their margins (Tarney, 1973) and is particularly common in the dolerite suite. However, some Assynt dykes sampled during this study were almost entirely fresh (particularly the picrite suite), displaying a primary igneous mineralogy. In the Rhiconich Terrane, the dykes have been pervasively deformed and amphibolitised during the Laxfordian, with the development of a strong and pervasive mineral foliation defined by aligned hornblendes. A similar mineral foliation can be observed in Laxfordian-age shear zones within the Assynt Terrane, and samples were collected from outside shear zones where possible.

The complex tectonometamorphic history of the area post-Scourie Dyke emplacement means that the effects of post-intrusion alteration must be considered. The chief controls on trace element mobility are the availability of fluid phases, the composition of the fluids (e.g., CO<sub>2</sub> or halogen-bearing fluids) and the type of alteration. Geochemical interpretations in this study are predominantly based on the elements generally regarded to be 'immobile' at low to moderate degrees of alteration and metamorphism, such as Th, Ti, P, Zr, Y, Nb and other high field strength elements (HFSE) (e.g., Jenner, 1996; Pearce, 1996). Early investigations of the Scourie Dykes (Weaver and Tarney, 1981a) suggested that element mobility only become significant after considerable recrystallisation, during which the large ion lithophile elements (LILE) were particularly mobile. In the absence of significant fluid-based alteration and circulation, rare earth elements (REE) appear to be stable up to granulite-facies metamorphism (Weaver and Tarney, 1981a; Jenner, 1996) and REE abundances in the Scourie Dyke Swarm are therefore unlikely to have been significantly affected by post-intrusion metamorphism. LILE such as Ba, K, Rb and Sr have also been tentatively used in geochemical interpretations of the dykes, despite their apparent mobility during metamorphism. These data are particularly relevant in light of the lack of LILE-rich host rocks in the Assynt Terrane, suggesting that any enrichment in these elements was a primary feature of the Scourie Dyke magma.

However, these mobile elements have not been used for modelling of magma fractionation. Finally, Platinum Group Elements (PGE) are effectively immobile in the absence of fluid-rich alteration (Gammons and Bloom, 1993; Crocket, 2000), so they are regarded in this study as relatively immobile. However Au is significantly more mobile during metamorphism and fluid-based alteration (Crocket, 2000), but is not directly used in interpretations in this study.

## 2.2. The Loch Roag mantle xenolith locality

Direct evidence about the lithospheric mantle beneath NW Scotland is limited to a few xenolith localities. One of these is a Tertiary monchiquite dyke (45.2 Ma; Faithfull et al., 2012) that intrudes the Lewisian Gneiss Complex near Loch Roag on the Isle of Lewis (Fig. 1b). This dyke contains numerous xenoliths, xenocrysts and megacrysts from the lower crust and lithospheric upper mantle (Faithfull et al., 2012). Previous detailed work has highlighted the metasomatised state of this region of lithospheric upper mantle (Upton et al., 1983, 2011; Menzies et al., 1987; Long et al., 1991). Sr, Nd and Pb isotopic analyses of the spinel lherzolite and pyroxenite xenoliths suggest the presence of an old, stable keel below the Lewisian Gneiss Complex, which has been enriched over a period of 1000–1500 Myr in incompatible elements, particularly Ba, Rb, Sr, P and the LREE (Menzies et al., 1987; Long et al., 1991). Time-integrated Nd and Sr isotope systematics indicate a geochemical enrichment event at ca. 2.5–2 Ga, involving interaction with carbonatite (Long et al., 1991). The only magmatic event known to have occurred within this time period is the intrusion of the Scourie Dykes, and thus the Loch Roag xenoliths may provide information about the source of these dykes.

## 3. Sampling and analytical methods

Samples were collected to include the picrite, olivine gabbro, and dolerite dyke varieties. In all, 50 samples were collected from 40 individual dykes for analysis of major and trace elements, and a representative selection of 25 samples were assayed for bulk rock PGE and gold (Appendix A). Most samples were collected from dyke centres to minimise effects of local crustal contamination, but some were also collected from dyke margins for comparison. The most common dolerite dykes were sampled from each of the three Lewisian Terranes (39 samples from the Assynt Terrane, 9 from the Gruinard Terrane, and 6 from the Rhiconich Terrane (Fig. 1)). The samples have been assigned to the dolerite, olivine gabbro, and picrite suites based on their petrology, mineralogy and geochemistry. The suite includes 4 olivine gabbro dyke samples, 6 picrites and 40 dolerite dykes.

Spinel lherzolite mantle xenolith samples from Loch Roag were provided by the British Geological Survey, including 4 rounded xenoliths approximately 3–6 cm in diameter. When cut, the peridotite xenoliths show mostly green alteration halos, with visible replacement-reaction textures in these areas. In some samples (e.g., LR80) a grey-black, relatively 'unaltered' central zone in the xenolith was cut out and analysed separately to its green halo. Overall these peridotite xenoliths are medium- to coarse-grained (crystals ranging 0.5–2 mm). Samples weighed at least 25–50 g (maximum available), to ensure that as large a sample as possible was homogenised for whole-rock geochemical analyses.

For the dyke samples, weathered material was removed from each sample before being crushed, split, and milled to a fine powder in an agate planetary ball mill at Cardiff University. Major and trace elements were analysed by inductively coupled plasma optical emission spectrometry (ICP-OES) and inductively coupled plasma mass spectrometry (ICP-MS), respectively, at Cardiff University using methods and instrumentation described by McDonald and Viljoen (2006). Samples were analysed for PGE and Au by Ni

sulphide fire assay followed by tellurium co-precipitation and ICP-MS (Huber et al., 2000; McDonald and Viljoen, 2006). Accuracy was constrained by analysis of the certified international reference materials TDB1 and WMG1 for PGE + Au, and JB1a for all other trace and major elements (see Appendix B). Precision was estimated by repeat analysis of a sub-set of samples (Appendix B). Representative data for each dyke suite are listed in Table 1. A full table of results is available in Appendix A.

For determination of rhenium-osmium abundances and isotopic composition, analyses were carried out at the TOTAL Laboratory at Durham University and follow the analytical procedures of Selby et al. (2009). Whole-rock powders were weighed and loaded into carius tubes with a known amount of spike solution ( $^{185}\text{Re} + ^{190}\text{Os}$ ) together with 9 mL of inverse *aqua regia*. Tubes were sealed and heated to 220 °C for 48 h.  $\text{CHCl}_3$  solvent extraction and micro-distillation isolated Os, and Re was separated using an anion exchange column and single-bead chromatography. Resulting Re and Os were loaded onto Ni and Pt filaments for isotopic analysis using negative-ion mass spectrometry on a Thermo Electron TRITON mass spectrometer. Results and uncertainties ( $2\sigma$ ) are presented in Table 3, and model age equations in Appendix C.

## 4. Scourie Dyke geochemistry

### 4.1. Major elements

All the analysed dykes contain <53 wt.%  $\text{SiO}_2$  and on an AFM diagram (Fig. 2a – anhydrous data plotted for all major element diagrams) they display an Fe-enriched tholeiitic trend. The total alkalis vs. silica (TAS) classification shows that most dykes fall within the basaltic field (Le Maitre et al., 2002), with some overlap into the picrumbasic, trachybasalt and basaltic andesite fields (Fig. 2b) and unusually high  $\text{SiO}_2$  contents in the picrites. Major element binary diagrams (anhydrous) plotted against  $\text{MgO}$  content (Fig. 2c–f) highlight clear separation between the dyke groups. These diagrams display considerable major element variability in the dolerites, particularly notable for  $\text{Fe}_{2\text{O}}_{3\text{T}}$ , CaO and  $\text{TiO}_2$ , due to fractional crystallisation of minerals such as olivine, pyroxenes, spinel and magnetite/ilmenite. The clustered  $\text{Al}_2\text{O}_3$  composition (Fig. 2c) of the dolerites indicates little or no plagioclase fractionation took place in the magma, therefore the variation of CaO in the dolerites is a response to clinopyroxene fractionation. Variable  $\text{K}_2\text{O}$  content of dolerites, with no clear corresponding variation for  $\text{Na}_2\text{O}$  (Appendix A), is likely due to the mobility of these elements during metamorphism and alteration. The picrite and olivine gabbro suites have low  $\text{TiO}_2$  (<0.7 wt.% and <2 wt.% in picrites and olivine gabbros, respectively), and low  $\text{Al}_2\text{O}_3$ ,  $\text{Na}_2\text{O}$ , CaO,  $\text{Fe}_{2\text{O}}_{3\text{T}}$  and  $\text{P}_2\text{O}_5$  concentrations in comparison to the dolerite suite, but substantially higher  $\text{MgO}$  contents. Picrite dykes contain >17 wt.%  $\text{MgO}$ , while olivine gabbro dykes contain 11–17 wt.%  $\text{MgO}$  (hydrous). While evidence of a fractional crystallisation trend is observed for the dolerites, the variability of major elements such as  $\text{Fe}_{2\text{O}}_{3\text{T}}$ , CaO and  $\text{TiO}_2$  with  $\text{MgO}$  for picrites and olivine gabbros is less clearly related to fractionation, with the exception of  $\text{Al}_2\text{O}_3$  for olivine gabbros, where plagioclase may have fractionated.

Despite some degree of mobility of  $\text{K}_2\text{O}$  and  $\text{Na}_2\text{O}$  during amphibolite facies metamorphism, picrites have <3 wt.% total alkalis ( $\text{Na}_2\text{O} + \text{K}_2\text{O}$ ), whilst the olivine gabbro and dolerite suites are considerably more variable with up to 5.2 wt.%  $\text{Na}_2\text{O} + \text{K}_2\text{O}$ . Loss on ignition (LOI wt.%) values do not vary systematically between dyke suites (see Table 1 and Appendix A) with most samples ranging from 0.25 to 3 wt.%. Finally, no systematic variation can be observed for the dolerite dyke group throughout the three Lewisian Terranes. Whole rock major element geochemical compositions of these samples do not vary according to the terrane in to which they were intruded.

### 4.2. Trace elements

All dyke suites are depleted in high field strength elements (HFSE). Mantle-normalised multi-element patterns (Fig. 3a–c) show a negative Nb-Ta anomaly, and the picrite suite also displays a trough at Ti (corresponding to  $\text{TiO}_2 < 1$  wt.%). Most dolerite dykes have a positive Ti anomaly and show Th enrichment, but a small sub-group of dolerite dykes display negative Ti anomalies, and more pronounced negative Nb-Ta anomalies (Fig. 3c). Most of the olivine gabbro dykes do not display a trough for Ti in the multi-element diagram (Fig. 3b) corresponding to  $\text{TiO}_2 = 1\text{--}2$  wt.%, but still show significant negative anomalies for Nb and Ta—a feature that could be reconciled by inferring Ti-magnetite accumulation. Rare dolerite dyke samples (e.g., X39 and X71) display very flat multi-element patterns. These samples have low to mid-range  $\text{K}_2\text{O}$  and Rb concentrations in comparison to other dolerite dykes, and coupled with their flat multi-element patterns (i.e., no Th enrichment, Nb-Ta-Ti trough) these may represent rare ‘uncontaminated’ asthenospheric magmas. However these dykes are also located in Laxfordian shear zones and show evidence of alteration textures as well as an increase in serpentine, talc or mica, indicating that they have been altered by fluids circulating in the shear zones.

All dyke suites are enriched in Th, LREE and LILE (Figs. 3 and 4) and have slight positive Zr-Hf anomalies (Fig. 3). The Th and some LILE enrichment of Scourie Dykes (e.g., Rb and K) is in stark contrast to the whole-rock geochemistry of the Lewisian granulite-facies TTG of the Assynt terrane, which is notably depleted in these elements. However, the amphibolite-facies gneisses of terranes to the north and south are less depleted in these elements (Fig. 3d and Fig. 4a and b). Both amphibolite- and granulite-facies gneisses are more enriched in Ba (Fig. 4c) and Sr than the dykes (Table 1 and Appendix A).

All dyke suites display chondrite-normalised rare earth element (REE) patterns that are enriched in the light REE (LREE) (Fig. 3e–g), but the dolerite dykes are most enriched with concentrations of La up to 100× chondrite values (Fig. 3g). The dolerite dykes have flatter middle REE (MREE) patterns, with no fractionation of the heavy REE (HREE), unlike that shown by the picrite and olivine gabbro suites. Overall, dolerites have the highest total REE concentrations. Picrites have the highest La/Sm ratio, while the olivine gabbro suite has the highest Gd/Yb. Variability in LREE of the olivine gabbros (Fig. 3f) could indicate fractionation of clinopyroxene. Picrites and olivine gabbros also have the highest Th/Yb ratios and olivine gabbros have the highest  $\text{TiO}_2/\text{Yb}$  ratios. Picrite dykes have the highest La/Nb and Ce/Sm ratios of all the dyke suites (Fig. 4d), but the olivine gabbro and dolerite suite are not distinguishable using these trace element ratios.

The different suites also have distinctive Co concentrations (up to 157 ppm and 72 ppm in picrites and dolerites, respectively). MgO and Ni concentrations are positively correlated between the three dyke groups (Fig. 4e) reflecting the observed olivine content of these dykes. Similarly this is the case for Ni and Co (Fig. 4f). However on close inspection, the dolerites tend to cluster (particularly for Co; Fig. 4f close-up) with no clear fractionation trend, suggesting little or no olivine fractionation within this suite. Further, there is a poor positive correlation ( $R^2 = 0.61$ ) between Ni and Co for the olivine gabbro and picrite suites together. It is possible that the broad positive Ni-MgO and Ni-Co trends for the Scourie Dykes indicate control by olivine crystallisation (particularly in the picrites). Overall, the geochemical compositions of the three dyke suites signal that they are not cogenetic and cannot be related to one another by a simple fractionation trend from the same magma source. Instead these indicate at least two, magma sources (dolerites vs. picrites, while olivine gabbros may be related by fractionation to the dolerites). No systematic variation can

**Table 1**

Scourie Dyke major and trace element whole-rock analyses for a representative selection of picrite, olivine gabbro, and dolerite dykes suites. Sample code: P (picrite), OG (olivine gabbro), D (dolerite), c (dyke centre) and m (dyke margin). Numbers 1–10 correspond to approximate locations marked on Fig. 1.

Sample	X23 P.4.c	X25 P.4.c	X26 P.4.c	X27 P.4.m	X68 P.10.c	X10 OG.1.c	X36 OG.5.c	X37 OG.6.c	X52 OG.7.c	X8 D.1.c	X12 D.3.c
Grid ref.	NC	NC	NC	NC	NC	NC	NC	NC	NG	NC	NC
1447	1451	1448	1487	0498	1548	1197	0741	9602	1473	1637	
2256	2283	2283	2395	2710	4474	1590	2105	9276	4488	4872	
(wt.%)											
SiO <sub>2</sub>	49.63	47.43	50.25	52.50	50.46	47.64	47.97	45.27	48.10	43.43	48.55
Al <sub>2</sub> O <sub>3</sub>	10.61	7.23	6.19	7.39	6.21	7.26	11.86	8.62	10.14	12.12	10.57
Fe <sub>2</sub> O <sub>3</sub> *	11.21	11.10	11.07	12.23	11.55	14.54	14.98	19.00	13.37	21.21	20.00
MgO	17.36	19.81	21.52	16.34	20.38	16.51	11.07	13.82	12.25	5.85	6.07
CaO	6.37	5.16	5.64	7.32	7.07	9.08	7.96	8.96	9.71	10.01	8.41
Na <sub>2</sub> O	2.22	0.47	1.22	1.37	0.76	1.56	3.32	2.34	2.52	2.43	2.02
K <sub>2</sub> O	0.69	1.03	0.46	0.76	0.00	0.12	0.77	0.52	0.28	0.40	0.77
TiO <sub>2</sub>	0.67	0.47	0.36	0.68	0.43	1.41	1.62	1.96	1.34	3.14	2.25
MnO	0.16	0.15	0.17	0.19	0.19	0.22	0.20	0.23	0.21	0.28	0.35
P <sub>2</sub> O <sub>5</sub>	0.11	0.07	0.05	0.10	0.05	0.12	0.21	0.11	0.12	0.22	0.24
LOI	2.06	6.88	2.54	1.18	2.07	0.62	0.36	0.25	1.44	0.31	1.00
Total	101.09	99.80	99.46	100.04	99.18	99.09	100.32	101.07	99.49	99.41	100.23
Mg#	0.79	0.81	0.82	0.76	0.81	0.74	0.65	0.64	0.70	0.41	0.42
(ppm)											
Sc	19	18	19	25	23	28	25	30	25	50	50
V	176	146	132	218	162	255	304	435	297	566	559
Cr	1918	3891	4432	2823	2949	1689	910	1294	965	33	106
Co	114	142	157	93	87	129	85	142	69	59	59
Ni	1261	1474	1587	909	1209	1213	709	844	801	70	115
Cu	112	167	54	42	66	139	122	131	90	88	57
Rb	22	31	12	22	1	1	18	12	4	10	25
Sr	258	109	155	78	12	135	332	200	199	149	169
Y	14	10	9	15	10	15	23	20	17	35	45
Zr	73	70	55	81	53	80	182	109	93	115	151
Nb	3.1	2.9	1.6	3.7	1.4	6.3	7.7	5.0	2.7	7.6	11.7
Ba	366	174	315	239	1	73	266	175	92	123	190
La	13.87	10.78	8.43	14.02	7.34	9.34	15.93	9.79	4.43	9.23	11.76
Ce	28.58	21.75	17.27	30.45	15.36	23.66	35.62	23.22	12.79	22.63	27.77
Pr	3.76	2.84	2.23	3.97	2.12	3.64	5.12	3.53	2.13	3.58	4.44
Nd	14.11	10.30	8.42	14.65	8.27	15.40	21.81	15.76	10.54	16.16	19.80
Sm	2.80	2.00	1.68	2.88	2.00	3.74	5.63	4.19	3.43	4.62	5.39
Eu	0.80	0.62	0.52	0.75	0.45	1.08	1.50	1.19	1.04	1.52	1.68
Gd	2.41	1.83	1.54	2.62	1.69	3.21	4.59	3.63	2.93	4.72	5.73
Tb	0.38	0.27	0.24	0.42	0.27	0.51	0.73	0.61	0.51	0.87	1.04
Dy	2.15	1.60	1.37	2.44	1.65	2.79	4.12	3.50	2.97	5.54	6.79
Ho	0.42	0.31	0.27	0.48	0.33	0.52	0.76	0.64	0.56	1.14	1.42
Er	1.20	0.91	0.81	1.38	0.95	1.41	2.04	1.75	1.49	3.38	4.29
Tm	0.18	0.13	0.11	0.20	0.13	0.19	0.26	0.23	0.20	0.49	0.61
Yb	1.15	0.88	0.75	1.23	0.88	1.15	1.59	1.44	1.27	3.08	4.08
Lu	0.17	0.13	0.11	0.19	0.14	0.17	0.27	0.23	0.18	0.50	0.66
Hf	1.66	1.85	1.18	1.89	1.21	2.40	4.45	3.31	2.71	3.10	4.02
Ta	0.21	0.21	0.09	0.19	0.11	0.46	0.49	0.28	0.21	0.41	1.05
Th	1.66	1.42	1.22	2.58	1.20	1.25	2.90	1.15	1.08	1.09	1.34
U	0.35	0.28	0.21	0.60	0.29	0.31	0.37	0.24	0.18	0.26	1.25
(ppb)											
Os	0.59	0.95	1.26	0.36	0.43	0.42	1.44	1.53	0.96	0.06	0.06
Ir	0.71	1.12	1.23	0.68	1.01	1.40	1.75	2.53	1.36	0.22	0.07
Ru	1.95	3.33	3.46	2.01	2.56	2.13	2.39	3.47	2.13	0.43	0.14
Rh	0.59	0.88	1.38	0.62	0.97	0.92	0.81	1.09	0.67	0.36	0.11
Pt	1.89	2.78	4.17	5.61	5.59	8.38	6.91	9.20	9.81	2.11	0.70
Pd	2.65	1.83	3.13	2.86	4.92	8.31	5.85	7.90	6.24	1.33	0.57
Au	1.23	12.31	1.17	1.43	0.82	3.26	1.50	2.17	1.70	1.20	1.75
Cu/Pd	42.4	90.9	17.4	14.7	13.5	16.7	20.9	16.6	14.4	66.4	100.0
Pd/Ir	3.7	1.6	2.5	4.2	4.9	5.9	3.3	3.1	4.6	5.9	7.7

**Table 1** (Continued)

X28 D.4.c	X31 D.4.c	X33 D.5.c	X34 D.5.c	X35 D.5.c	X39 D.6.c	X40 D.2.m	X44 D.7.c	X50 D.7.c	X53 D.8.c	X58 D.9.c	X69 D.10.c	X71 D.10.c
NC	NG	NG	NC	NC	NC	NC						
1698	1717	1197	1197	1201	0820	1455	9867	9552	2481	2409	0498	0593
2581	2602	1605	1605	1606	2057	4161	9240	9044	4691	4979	2712	2510
51.12	51.07	50.59	50.30	50.41	47.92	51.13	50.05	51.94	50.67	52.05	49.38	48.01
15.13	12.86	12.83	12.88	12.94	12.31	13.13	9.57	12.56	13.06	12.76	13.23	13.43
10.17	17.19	15.63	16.51	16.84	18.61	15.83	14.60	14.02	14.05	16.04	15.26	14.70
6.37	4.89	5.27	5.10	5.28	6.64	5.39	10.00	6.30	5.09	4.72	6.64	7.08
10.60	8.23	9.17	8.50	9.23	7.60	8.86	9.57	11.45	8.10	7.52	11.10	11.21
3.07	3.00	2.40	2.57	2.54	3.16	2.43	2.39	1.80	3.42	2.74	1.69	1.80
0.65	0.66	0.66	0.73	0.70	0.71	0.69	0.72	0.40	1.71	1.03	0.78	0.42
0.71	1.63	1.70	1.82	1.90	1.79	1.75	1.49	1.52	1.75	2.01	1.77	1.18
0.18	0.27	0.24	0.24	0.24	0.28	0.23	0.22	0.22	0.25	0.23	0.23	0.22
0.07	0.18	0.17	0.17	0.20	0.11	0.29	0.18	0.13	0.16	0.22	0.14	0.08
0.99	0.77	0.31	0.43	0.31	1.96	0.70	1.46	0.89	1.00	2.04	0.66	0.93
99.06	100.73	98.97	99.25	100.58	101.09	100.44	100.26	101.23	99.27	101.37	100.89	99.07
0.61	0.41	0.46	0.43	0.44	0.46	0.46	0.63	0.53	0.48	0.43	0.52	0.54
32	38	42	40	42	48	37	24	42	38	36	41	41
250	410	450	388	429	556	341	234	444	325	460	353	326
320	56	160	126	151	186	61	837	58	24	19	62	129
48	60	59	51	54	68	48	73	57	45	45	49	53
161	99	93	77	89	93	261	323	85	55	23	83	129
56	164	196	149	185	1055	125	143	314	103	45	127	119
6	15	19	19	21	15	7	19	5	61	26	9	3
339	218	173	175	166	132	262	271	141	316	148	199	169
20	37	41	39	43	31	34	32	31	31	37	22	24
65	153	174	131	188	93	183	256	96	161	161	91	68
3.5	7.8	7.9	7.8	8.6	4.4	8.3	16.5	5.8	12.8	6.6	8.9	3.7
261	159	227	249	255	168	240	322	79	302	147	253	115
12.92	12.00	15.15	14.42	17.03	5.34	22.67	24.38	9.10	13.71	12.06	9.84	3.65
29.31	27.41	34.16	32.67	38.35	13.83	49.13	54.09	20.77	31.58	26.48	23.18	9.60
4.08	4.04	4.95	4.83	5.65	2.31	6.85	7.67	3.12	4.52	3.70	3.46	1.61
15.72	17.66	21.07	20.53	23.54	11.13	27.50	30.69	13.26	18.82	15.41	14.82	7.81
3.29	4.83	5.27	5.60	6.07	3.62	6.34	7.16	3.95	4.82	4.40	3.91	2.71
1.13	1.52	1.49	1.49	1.56	1.10	1.60	1.62	1.06	1.27	1.23	1.17	0.85
3.10	4.74	5.42	5.24	5.81	3.74	5.36	6.26	3.76	4.12	4.36	3.32	2.64
0.51	0.87	0.96	0.92	1.03	0.72	0.86	0.96	0.67	0.72	0.84	0.56	0.52
3.15	5.67	6.10	6.19	6.67	4.86	5.19	5.53	4.39	4.45	5.45	3.47	3.64
0.64	1.15	1.28	1.25	1.34	1.02	1.04	1.06	0.91	0.93	1.14	0.68	0.77
1.85	3.44	3.80	3.72	4.03	2.92	3.06	2.99	2.74	2.76	3.49	1.97	2.33
0.27	0.48	0.57	0.54	0.58	0.43	0.43	0.41	0.39	0.40	0.51	0.28	0.34
1.84	3.38	3.87	3.58	3.92	2.84	2.89	2.62	2.63	2.69	3.48	1.81	2.31
0.28	0.51	0.59	0.59	0.64	0.49	0.47	0.41	0.43	0.42	0.53	0.28	0.36
1.53	3.79	4.15	3.60	4.82	2.49	4.49	6.12	2.95	3.71	4.09	2.62	1.72
0.22	0.49	0.44	0.37	0.44	0.27	0.44	0.85	0.33	0.71	0.38	0.53	0.19
0.39	1.79	2.12	1.96	2.31	0.82	2.93	3.81	1.24	2.00	2.49	1.14	0.38
0.12	0.35	0.52	0.56	0.60	0.25	0.67	1.27	0.34	0.70	1.84	0.30	0.09
0.07	0.05	0.09	0.05	0.04	0.05	0.05	0.07	0.06	0.09	0.10	0.06	0.04
0.14	0.07	0.08	0.08	0.05	0.07	0.06	0.27	0.08	0.09	0.09	0.11	0.06
0.57	0.11	0.18	0.13	0.27	0.16	0.13	0.64	0.29	0.25	0.27	0.28	0.17
0.24	0.10	0.23	0.28	0.22	0.41	0.15	0.18	0.57	0.26	0.13	0.57	0.58
2.99	0.92	3.58	5.42	3.30	2.30	1.90	2.31	5.73	7.61	2.45	11.55	8.58
3.56	0.78	2.73	4.96	3.31	3.27	1.48	2.21	5.94	9.31	1.64	10.98	12.18
2.12	0.70	1.06	1.42	1.01	1.45	1.45	0.61	3.48	1.06	0.68	3.70	6.02
15.6	209.7	71.9	30.1	55.7	322.9	84.4	64.6	52.9	11.1	27.7	11.5	9.8
24.9	11.5	34.6	63.1	73.5	44.0	26.9	8.3	74.7	105.7	18.3	96.3	221.3

be identified in the trace element abundances of dolerite dykes intruded into the three mainland Lewisian terranes.

Total PGE + Au concentrations range from 38.3 ppb (olivine gabbro) to 2.7 ppb (dolerite). All dyke suites display fractionated chondrite-normalised PGE profiles (Fig. 5a-d) enriched in palladium-group PGE (PPGE) and the dolerite suite has notable iridium-group PGE (IPGE) depletion. The picrite and olivine gabbro dykes have relatively flat PGE + Au patterns, although these are still slightly fractionated. The picrites and olivine gabbro suites have significantly higher concentrations of Ni, Cr and Co than the dolerites, whilst Cu concentration varies widely across and within the dyke suites. This variation in Cu is predominantly due to its fractionation as an incompatible element in silicate magma.

Chalcophile element ratios, such as Cu/Pd, are typically higher than primitive mantle ratios. There is little consistent variation in Cu/Pd between dyke suites, although olivine gabbros tend to have the most primitive values (Fig. 5e). [Pd/Ir]<sub>N</sub> ratios from all the dyke suites are higher than typical mantle values (PRIMA (primitive mantle) ~0.97) and those from dolerite dykes are significantly higher than those in both picrites and olivine gabbro dykes (Fig. 5f). There is no correlation between dyke alteration (using Alteration Index =  $(K_2O + MgO)/(Na_2O + K_2O + CaO + MgO)^{1/2} \times 100$  (Ishikawa et al., 1976), LOI wt.%, and extent of amphibolitisation as a qualitative proxy) and PGE concentrations, suggesting that PGE were immobile during alteration and metamorphism and that variation in PGE geochemistry between dykes is a primary feature (Appendix B – Figs. (a) and (b)).

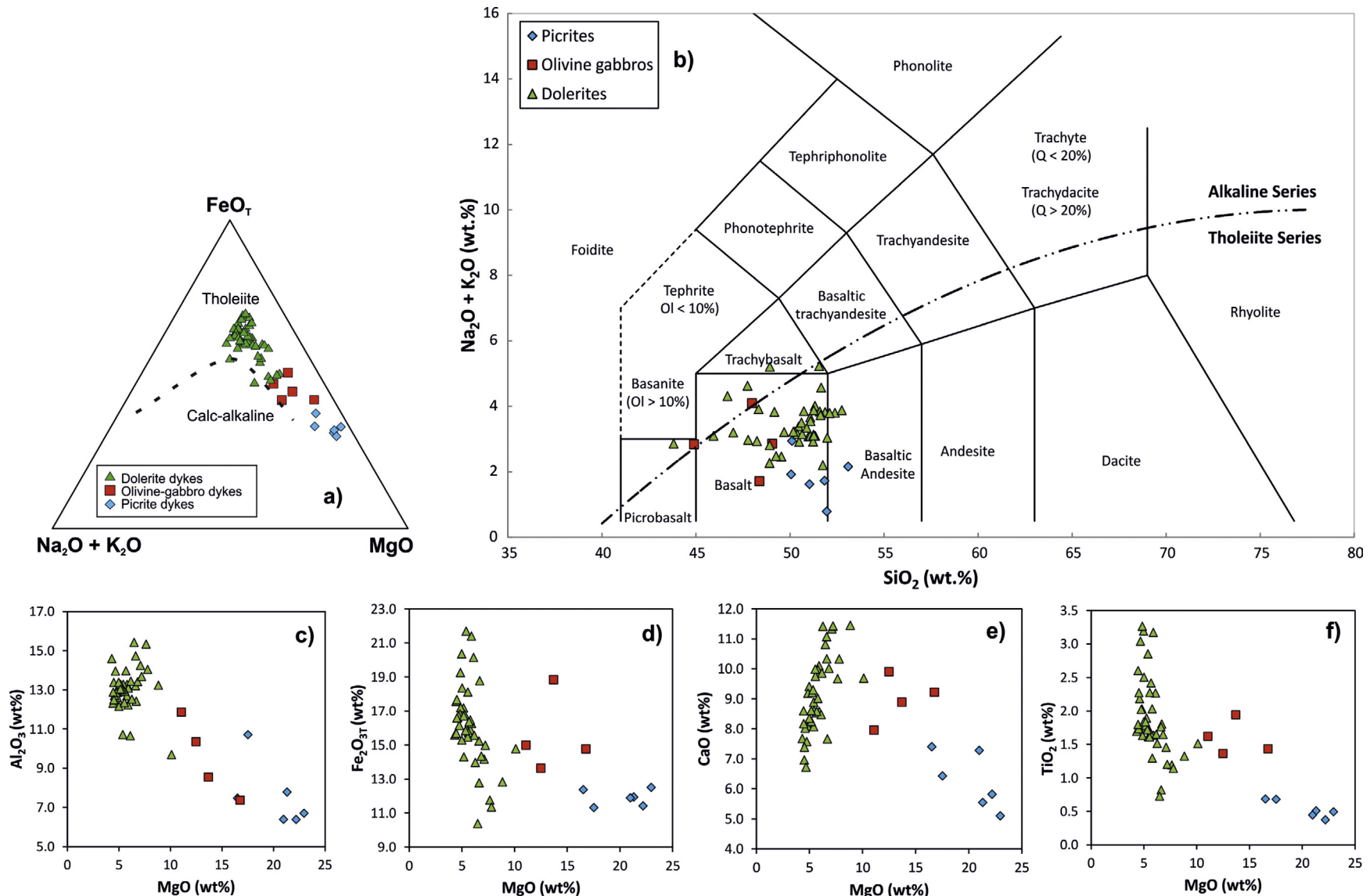


**Fig. 2.** Major element plots (anhydrous). (a) AFM classification of Scourie Dyke Suite.  $\text{Fe}_2\text{O}_{3T}$  where  $T$  denotes total iron.  $\text{FeO}_T$  in AFM diagram was converted from analysed  $\text{Fe}_2\text{O}_{3T}$  (total iron).  $\text{FeO}$  for use in calculating Mg-number (Mg#) was calculated by assuming actual  $\text{Fe}_2\text{O}_3$  ( $\text{Fe}_2\text{O}_3^*$ ) content = 1.5 +  $\text{TiO}_2$ . Then,  $\text{FeO} = (\text{Fe}_2\text{O}_{3T} - \text{Fe}_2\text{O}_3^*)/1.1$ . (b) Total alkali silica (TAS) classification diagram. (c)–(f) Major elements versus MgO (wt%). Note that all major element abundances have been recalculated as anhydrous for use in diagrams of Fig. 2. Concentrations cited in the main text are hydrous, for comparison to Table 1.

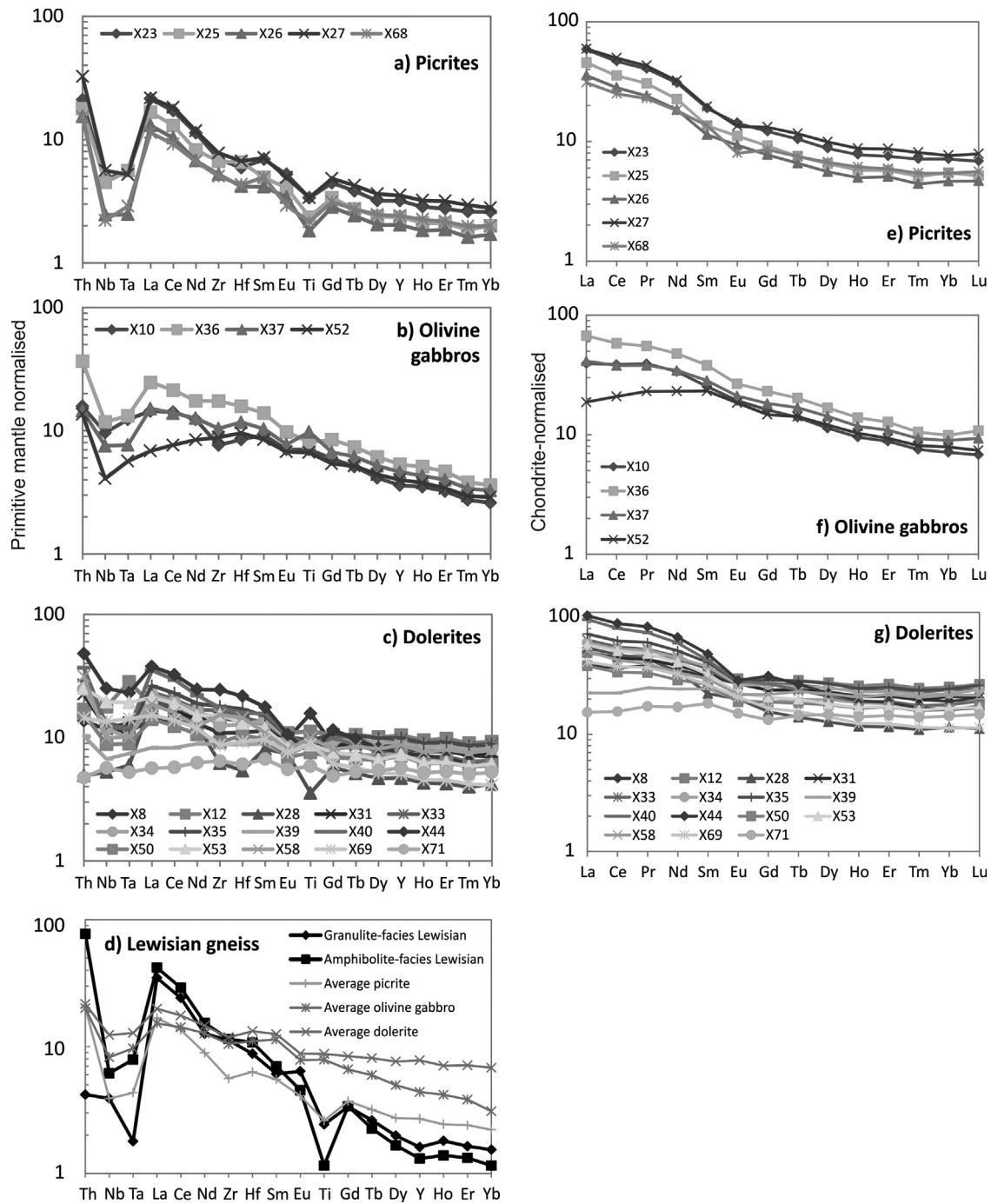


**Fig. 3.** (a)–(c) Multi-element normalised diagrams for each dyke suite. Plots are primitive mantle normalised (McDonough and Sun, 1995). (d) Comparison plot with Rollinson (2012) average granulite- and amphibolite-facies gneiss. (e)–(g) Chondrite-normalised (McDonough and Sun, 1995) rare earth element multi-element diagrams per dyke suite.

## 5. Mantle xenolith petrology and geochemistry

The Loch Roag spinel lherzolite mantle xenoliths consist of olivine, clinopyroxene, orthopyroxene and spinel, with accessory sulphides (mostly chalcopyrite, with some pentlandite). A Pt-sulphide grain ( $\sim 3 \mu\text{m}$  diameter) has been observed at the margin of a chalcopyrite droplet in LR80. Major silicate mineral phases are equigranular, with minor interstitial Fe-Ni-Cu sulphides (generally up to  $150 \mu\text{m}$  diameter). Samples are generally fresh, with fresh olivine throughout (particularly in the grey centres – e.g., sample LR80). On the outer rims of the xenoliths, a green rim of partial alteration is observed (generally 2–5 mm in width), in which

replacement reaction textures are more prevalent, and sulphides tend to be absent, but there are rounded barite-filled vugs. In sample LR80, this outer green material was easily removed, and thus the powdered sample was the most pristine (thus used for trace element geochemical modelling later in the paper). For more detailed descriptions of these samples, and their mineral chemistry, see Upton et al. (2011) and references therein.

Table 2 shows the first whole-rock geochemical analyses of the Loch Roag peridotite xenoliths. Their MgO contents (anhydrous) vary from 36.7 to 39.4 wt.% (comparable to primitive mantle composition (McDonough and Sun, 1995)).  $\text{Fe}_2\text{O}_3\text{T}$  is slightly elevated in comparison to primitive mantle, ranging from 10.3 to 11.9 wt.%

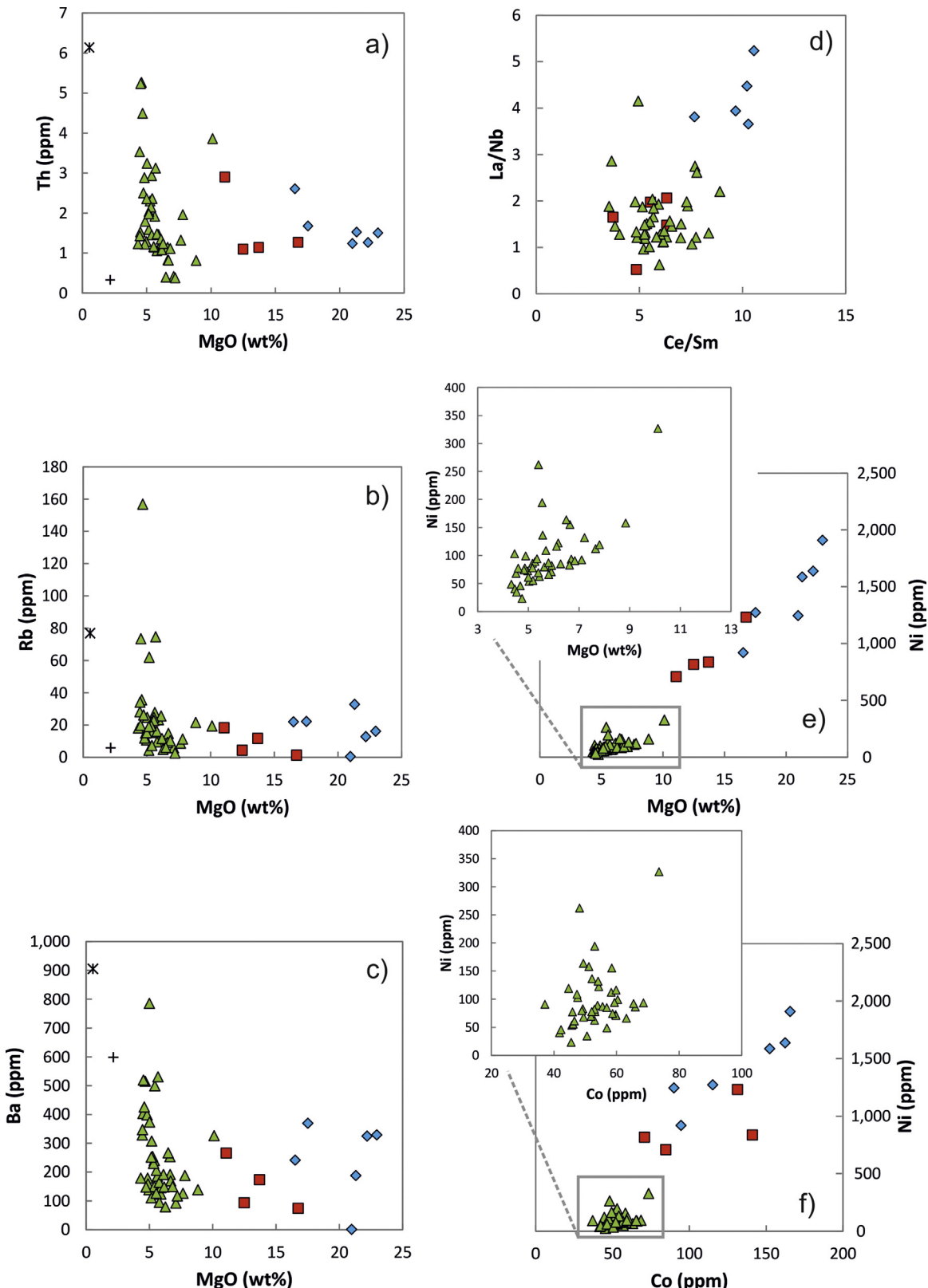


**Fig. 4.** Trace element plots. (a) Th-MgO and (b) Rb-MgO showing LILE enrichment of Scourie Dyke Suite relative to granulite-facies Lewisian TTG (plus sign) except for (c) Ba-MgO. Amphibolite-facies Lewisian gneiss also shown for reference (star). All Lewisian gneiss data is averaged from Rollinson (2012). (d) La/Nb-Ce/Sm bivariate plot to assess garnet-bearing component of source for the dyke suites. (e) and (f) show Ni and Co vs. MgO (anhydrous, wt.%). Inset plots for both (e) and (f) are close-up views for dolerite dyke data only.

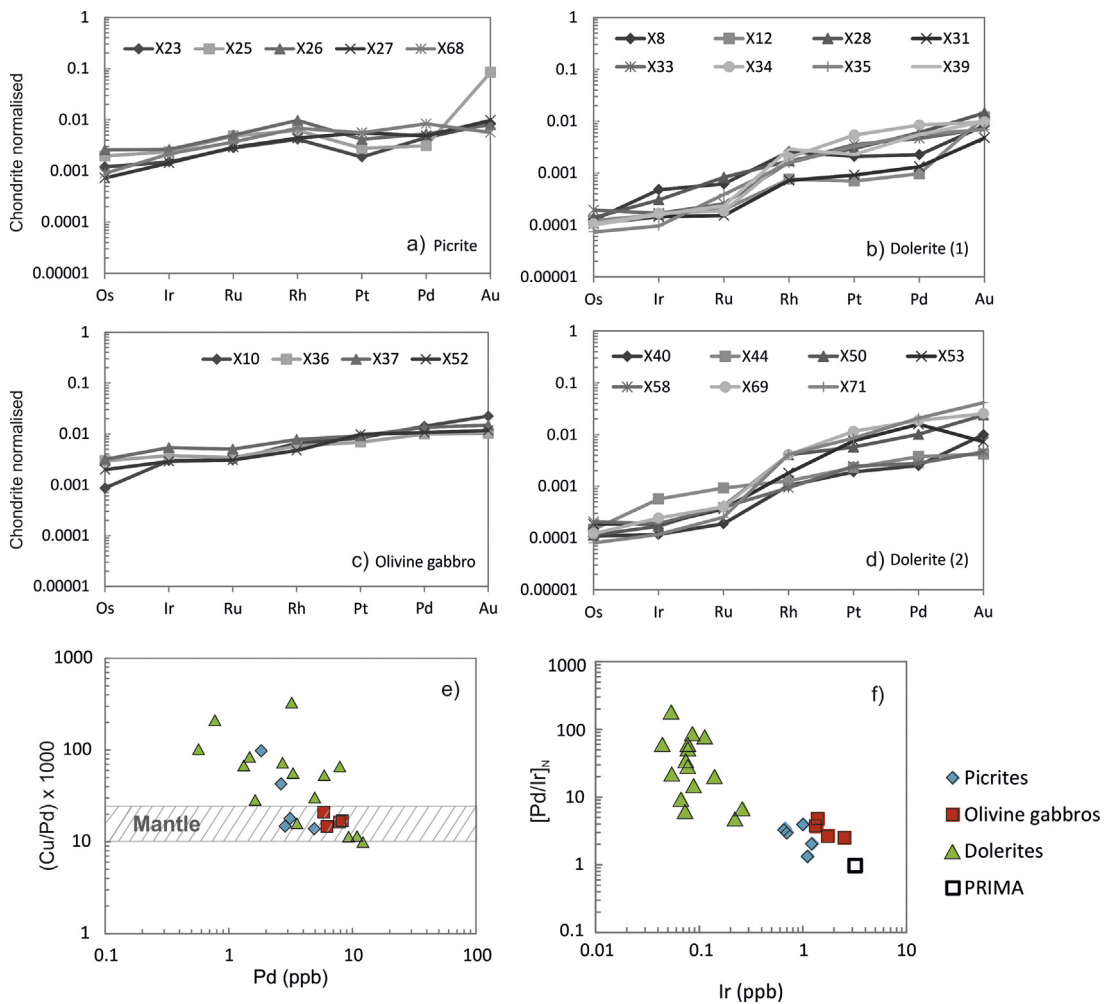


**Fig. 5.** (a)–(d) Platinum group element multi-element plots (chondrite normalised using McDonough and Sun, 1995) for picrite dykes, olivine gabbros, and dolerite dykes. (e) and (f) Platinum group element bivariate plots. Hatched area in (e) indicate typical mantle ratios for Cu/Pd. (f)  $[\text{Pd}/\text{Ir}]_N$  is chondrite-normalised Pd/Ir ratio. PRIMA is typical  $[\text{Pd}/\text{Ir}]_N$  for primitive mantle (McDonough and Sun, 1995).

(anhydrous), but  $\text{Al}_2\text{O}_3$  (1.1–2.5 wt.%) and  $\text{CaO}$  (2.3–2.7 wt.%) are lower than primitive mantle and  $\text{Ti}$  is significantly depleted, (only 13 to 30% of  $\text{Ti}$  in primitive mantle). This depletion in  $\text{CaO}$  and  $\text{Al}_2\text{O}_3$  may indicate partial melting and depletion of the mantle (by initial melting of clinopyroxene), which was subsequently re-enriched. But this would have caused an increase in  $\text{MgO}$  above primitive mantle levels which is not observed in these xenoliths, and coupled with their abundant clinopyroxene, makes this an unlikely scenario.

$\text{Nb}$  and  $\text{Ta}$ ,  $\text{Zr}$  and  $\text{Hf}$ , and  $\text{Ti}$  show negative anomalies (Fig. 6a) when normalised to primitive mantle, however  $\text{Nb}$  and  $\text{Ta}$  are not depleted below primitive mantle concentrations (i.e., not  $<1$  when normalised). HREE are not depleted either, but show flat trends similar to primitive mantle concentrations.  $\text{Zr}$ ,  $\text{Hf}$  and  $\text{Ti}$  are however  $<1$  on Fig. 6a. In contrast,  $\text{Th}$  and the LREE and MREE are markedly enriched to levels many tens of times more abundant than in primitive mantle (Fig. 6a). Chondrite normalised REE patterns (Fig. 6b) show a consistent negative Eu anomaly, or positive Gd anomaly. PGE and Au analyses indicate that the lithospheric mantle below this region of NW Scotland is fertile for these elements. Primitive mantle estimates for Au and Pd are 1 and 3.9 ppb, respectively (McDonough and Sun, 1995), but the Loch Roag xenoliths contain 2.0–3.3 ppb Au, and 4.7–11.5 ppb Pd. Pt is also elevated (11–16.9 ppb, compared with 7 ppb for primitive mantle) suggesting that the PGE and Au underwent enrichment, in addition to

Th, LILE and LREE. Finally the IPGE occur in concentrations comparable to primitive mantle, with Ir concentrations ranging from 2.9 to 3.6 ppb. This gives a slightly positive trend to the PGE + Au multi-element diagram (Fig. 6c), with enrichment in PPGE, but no depletion in IPGE.

## 6. Re-Os isotopes

Three whole-rock samples were analysed for Re and Os abundances and isotopic composition. This included two Scourie Dykes (X8 – the dolerite ‘Graveyard dyke’; and X23 – a picrite dyke from the north shore of Loch an Leathaid) and the freshest spinel lherzolite xenolith sample from Loch Roag (LR80). Results are displayed in Table 3, and calculated parameters include  $\text{Os}_i$  (initial  $^{187}\text{Os}/^{188}\text{Os}$ ),  $\gamma\text{Os}$  (calculated from the initial  $^{187}\text{Os}/^{188}\text{Os}$  and  $^{187}\text{Re}/^{188}\text{Os}$  ratios),  $T_{\text{MA}}$  (model age using Re/Os and assumed chondritic initial values),  $T_{\text{RD}}$  (Re-depletion Os model age assuming all Re is metasomatic) and  $T_{\text{RD}}^{\text{erupt}}$  (Re-depletion model eruption age assuming all Re is metasomatic and calculated prior to the time of eruption). In Table 3, \*Age are based on various published geochronology sources for the age of eruption (see caption). For further details, refer to the Appendix. X8 and X23 were analysed for comparison to earlier data collected by Frick (1998), in the light of new Re-Os methodologies and modern dating of the Scourie Dykes (Davies and Heaman,

**Table 2**  
Loch Roag major and trace element whole-rock analyses.

Sample	LR80	LR81	LR289	LR101335
(wt.%)				
SiO <sub>2</sub>	45.33	45.34	43.97	42.85
Al <sub>2</sub> O <sub>3</sub>	1.59	2.40	1.89	1.06
Fe <sub>2</sub> O <sub>3</sub> *	10.20	10.12	10.05	11.48
MgO	38.71	35.78	37.04	38.16
CaO	2.22	2.54	2.53	2.61
Na <sub>2</sub> O	0.44	0.46	0.30	0.16
K <sub>2</sub> O	0.09	0.54	0.11	0.03
TiO <sub>2</sub>	0.03	0.03	0.06	0.05
MnO	0.13	0.16	0.17	0.25
P <sub>2</sub> O <sub>5</sub>	0.04	0.15	0.12	0.22
LOI (%)	0.92	3.25	3.29	2.37
Total	99.70	100.78	99.53	99.23
(ppm)				
Sc	12	13	12	9
V	47	60	48	37
Cr	2427	2935	3047	2607
Co	104	112	132	131
Ni	2117	1743	2015	2331
Cu	175	90	101	66
Rb	2	6	3	1
Sr	28	256	250	94
Y	4	7	9	10
Zr	6	5	7	16
Nb	1.1	0.4	1.0	3.4
Ba	13	48	38	26
La	18.91	100.23	87.14	54.65
Ce	21.13	216.44	213.27	135.63
Pr	2.74	15.96	20.02	12.26
Nd	7.89	40.74	53.41	35.78
Sm	0.93	4.36	6.47	4.72
Eu	0.22	0.75	1.12	0.93
Gd	0.82	3.59	4.80	3.78
Tb	0.10	0.33	0.47	0.41
Dy	0.58	1.39	2.11	2.00
Ho	0.11	0.22	0.34	0.32
Er	0.32	0.64	0.97	0.89
Tm	0.05	0.09	0.14	0.13
Yb	0.32	0.54	0.87	0.78
Lu	0.05	0.08	0.13	0.11
Hf	0.14	0.14	0.17	0.42
Ta	0.07	0.02	0.06	0.19
Th	1.26	2.71	2.81	0.89
U	0.33	0.73	1.02	0.24
(ppb)				
Os	3.45	2.75	3.63	3.29
Ir	3.60	3.08	3.64	3.48
Ru	6.03	5.79	6.41	5.77
Rh	1.47	1.35	1.68	1.54
Pt	16.88	12.52	11.07	11.69
Pd	11.48	6.35	4.70	5.00
Au	1.96	2.28	3.30	2.00

2014). LR80 was run as an unknown sample, with no previous Re-Os data for the Loch Roag mantle xenoliths available in the literature.

For the two dykes, X8 has significantly higher Re and Os abundances than X23 (3.4 vs 0.4 ppb and 1090 vs. 108 ppt, respectively). Therefore X8 has high <sup>187</sup>Re/<sup>188</sup>Os and very radiogenic Os<sub>i</sub> and γOs, suggesting significant disturbance of the isotopic system, post-intrusion. This is comparable to previous measurements of the 'Graveyard dyke' by Frick (1998). In contrast picrite dyke X23 has γOs = -6.73 and Os<sub>i</sub> = 0.104 (lower than the predicted mantle range of 0.11–0.50 at 2400 Ma), and its <sup>187</sup>Re/<sup>188</sup>Os and <sup>187</sup>Os/<sup>188</sup>Os are within the range of results by Frick (1998).

The Os<sub>i</sub> (0.127) and γOs (-0.94) of xenolith LR80 has been calculated at 45.2 Ma, based on the age of the host dyke at Loch Roag (Faithfull et al., 2012). However, Long et al. (1991) used time integrated Nd-isotopes to suggest there was a major metasomatic event between 2.3 and 2.5 Ga and 1.0–1.5 Ga. If we recalculate Os<sub>initial</sub> for LR80 at 2.4 Ga, this is 0.07 – a result too unradiogenic for mantle at

**Table 3**  
Re-Os isotope data (whole-rock) for dolerite dyke (X8 – 'the Graveyard Dyke'), picrite dyke (X23) and Loch Roag spinel lherzolite xenolith (LR80). Calculated parameters include Os<sub>i</sub> (initial <sup>187</sup>Os/<sup>188</sup>Os), γOs (calculated from the initial <sup>187</sup>Os/<sup>188</sup>Os and <sup>187</sup>Re/<sup>188</sup>Os ratios), T<sub>MA</sub> (model age using Re/Os and assumed chondritic initial values), T<sub>RD</sub> (Re-depletion Os model age assuming all Re is metasomatic) and T<sub>RD</sub><sup>exp</sup> (Re-depletion model eruption age assuming all Re is metasomatic and calculated prior to the time of eruption). In Table 3 <sup>187</sup>Os/<sup>188</sup>Os initial (Os<sub>i</sub>) is calculated from eruption ages as indicated (\*Age). Age are based on various published geochronology sources for the age of eruption. Note that dykes ages from U-Pb isotopic ages from Davies and Heaman (2014) for X8 (Graveyard Dyke) and X23 (Cnoc an Leathaid). Eruption age of LR80 based on <sup>40</sup>Ar/<sup>39</sup>Ar date (Faithfull et al., 2012). All uncertainties reported to 2 s.d. level, all data are blank corrected. Blanks for Re and Os are 1.3 pg and 0.1 pg, respectively, and mean <sup>187</sup>Os/<sup>188</sup>Os of 0.173. For model age equations, refer to Appendix C.

Sample/Batch	Rock type	Re (ppb) total	±	Os (ppt) total	±	<sup>187</sup> Re/ <sup>188</sup> Os	±	<sup>187</sup> Os/ <sup>188</sup> Os	±	*Age (Myr)	T <sub>MA</sub> (Myr)	T <sub>RD</sub> (Myr)	T <sub>RD</sub> <sup>exp</sup> (Myr)	
X8/R0338-7	Dolerite dyke	3.42	0.02	108.3	5.5	1784.8	135.1	82.3096	7.0381	0.882	9.731	8655.01	2391.7	—
X23/R0538-9	Picrite dyke	0.40	0.01	1089.9	19.5	1.8	0.1	0.1767	0.0100	0.566	0.103	-7.24	2418.0	2080
LR80/R0538-8	Spinel lherzolite xenolith	0.51	0.01	1755.2	31.2	1.4	0.1	0.1278	0.0072	0.609	0.127	-0.94	45.2	-28

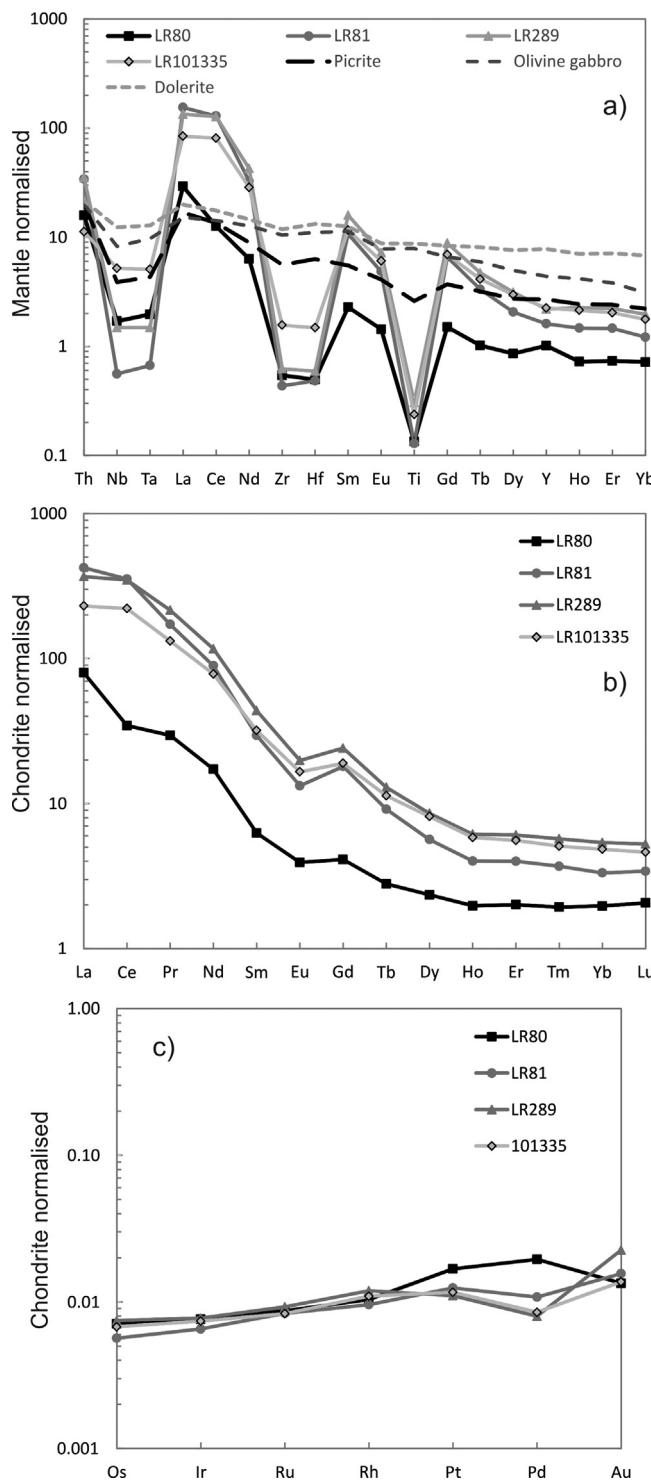


**Fig. 6.** Loch Roag multi-element diagrams: (a) primitive mantle normalised trace element multi-element diagram, (b) REE chondrite-normalised plot, and (c) chondrite-normalised PGE + Au plot.

that time, and suggesting that the Re-Os system has been disturbed slightly.

## 7. Discussion

The geochemistry of the mafic and ultramafic rocks of the Scourie Dyke swarm fits with structural and metamorphic observations, and the commonly accepted view that these magmas were

derived from the mantle during extension (Tarney and Weaver, 1987; Bridgwater et al., 1995; Park, 1995), and intruded into the Lewisian lower to middle crust. On the basis of the new geochemical data several further inferences can be made about the mantle sources of these dykes and the mantle beneath the Lewisian gneiss Complex at the time of their formation.

### 7.1. Dyke composition in relation to Lewisian terrane

Although the compositions of the doleritic Scourie Dyke swarm are variable, no systematic geochemical difference was observed across the three Lewisian terranes (Rhiconich, Assynt and Gruinard). Picrite and olivine gabbro dykes are rare in the granulite facies Assynt Terrane, and absent in the amphibolite facies Gruinard and Rhiconich Terranes to the south and north. This may be due to the depth of current erosion levels across the Lewisian terranes. The granulite-facies Assynt Terrane is considered to represent the lower crust (Park and Tarney, 1987), while the amphibolite-facies terranes represent mid-crustal levels. The absence of picrite and olivine gabbro dykes from the amphibolite-facies terranes might imply that these more MgO-rich magmas did not ascend as high into the crust, becoming trapped in lower crustal regions. Their elevated MgO contents imply their parental magmas were considerably denser than the dolerite dyke magmas, restricting their ascent. In addition, the homogeneity of the dolerite dyke suite across the three Lewisian terranes suggests that these Lewisian blocks had been accreted onto each other before dyke intrusion, confirming the conclusions of Goodenough et al. (2010), and supporting those of Davies and Heaman (2014). However this excludes the dykes at Shieldaig near Gairloch, which occur south of the Loch Maree Group (itself accreted in an arc setting after c. 1900 Ma; Park, 2002).

### 7.2. Mantle melting regime – evidence of crustal contamination or SCLM melting?

The ultimate mantle source of the Scourie Dyke magmas could potentially be either the convecting asthenosphere or the sub-continental lithospheric mantle. Enriched LREE patterns and trace element ratios indicate that dyke suites were derived from a mantle source with significantly higher LILE concentrations than the Lewisian TTG of the Assynt terrane (Rollinson, 2012). The high La/Sm ratio of picrite dykes in particular is suggestive of a relatively enriched mantle source, while the high Gd/Yb of olivine gabbros and picrites (relative to the dolerite suite) could indicate a comparatively deep garnet-bearing source region, or at least a source with a garnet-like signature, irrespective of actual depth. HREE patterns in the dolerite dyke suite are flatter ( $[Gd/Yb]_N$  generally <1.5; Fig. 3g) likely due to an absence of garnet in the source (i.e., in the spinel lherzolite stability field).

In order to test the possible mantle sources, trace element modelling is used. Details of the methods, equations, conditions and geochemical parameters used in the modelling presented below are provided in Appendix B. A summary of modelling parameters is given in Table 4.

#### 7.2.1. Dolerite dykes

Trace element modelling based on recent asthenospheric type sources (e.g., primitive mantle (PM), and enriched mantle EM1 and EM2) was initially employed. Partial melting was used for the dolerite dyke suite. As a starting point, modelling of 30% partial melting of a spinel lherzolite primitive mantle source (McDonough and Sun, 1995) with 45–50% fractional crystallisation of olivine was attempted; however this cannot replicate the trace element composition of the dolerite dykes. Fractional crystallisation of various modal proportions of olivine, orthopyroxene, clinopyroxene,

**Table 4**

Parameters required for melting, mixing, contamination, and fractional crystallisation during dyke magma evolution.  $F$  is % partial melting,  $r$  is % ratio of assimilation rate to fractional crystallisation, and  $x$  is % of contaminant added to primary melts in binary mixing model. Percentage olivine fractional crystallisation provided (ol. FC). Mantle sources used include primitive mantle† ([McDonough and Sun, 1995](#)), enriched mantle (EM1)‡ ([Willbold and Stracke, 2006](#)) and depleted mantle (DMM)\*\*\* ([Workman and Hart, 2005](#)). Lewisian contaminants\* ([Rollinson, 2012](#)) and SCLM partial melts\*\*, based on fresh xenolith material of sample LR80 (see [Table 2](#)).

Dyke suite	Mantle source modelled (non-batch melting)	% partial melting ( $F$ ) asthenos.	% partial melting ( $F$ ) lithos (SCLM)	% mixing (binary mixing model)
Dolerite	Spinel lherzolite DMM** asthenospheric melt + spinel lherzolite SCLM melt (based on LR80)	c. 2%	15% LR80 melt	$x = 0.1\text{--}0.3$
Picrite	Garnet lherzolite DMM** asthenospheric melt + spinel lherzolite SCLM melt (based on LR80)	c. 10%	30% LR80 melt	$x = 0.2\text{--}0.4$

plagioclase, and accessory minerals including magnetite and rutile, also failed to reproduce the multi-element patterns of the dolerites without invoking an unreasonably high degree of crystal fractionation (>80%) for a poorly acceptable model fit. Modelling using an enriched mantle source (EM1) – potentially more fitting to the Scourie dolerite dyke geochemistry – produces a similarly poor fit to multi-element spectra. In particular, modelling using either PM or EM1 sources is unable to replicate the characteristic anomalies for Th, Nb, Ta and Ti in the dolerites. Overall, this implies that the dolerites have experienced some degree of lithospheric contamination, either involving the crust or SCLM, or that the source regions of the parental magmas are significantly different from more recent asthenospheric compositions used in modelling.

The dolerite suite can be subdivided into two broad groups – high- $\text{TiO}_2$  (> 2 wt.%, with positive Ti-anomaly) and low- $\text{TiO}_2$  group (<2 wt.%, with negative Ti-anomaly) ([Fig. 3g](#)). Geochemical modelling cannot replicate this positive Ti anomaly using any realistic contamination components, and the presence for the Ti anomaly does not consistently coincide with any effect for Nb or Ta. High-Ti dolerite dykes commonly have higher Fe contents (>17 wt.%  $\text{Fe}_2\text{O}_{3T}$ ) and this might suggest a higher magnetite and/or ilmenite content.

AFC modelling using Lewisian amphibolite-facies gneiss ([Rollinson, 2012](#)) as the contaminant with low to moderate rates of assimilation ( $r = 10\text{--}20\%$ ) and fractionation of 40–65% olivine, can successfully reproduce the trace element signature of the dolerite dykes from a 30% melt of a spinel lherzolite primitive mantle (PM) source ([Fig. 7a and b](#)). Indeed, lower degrees of partial melting of this source (10–25%) can still successfully replicate the range of dolerite dyke trace element compositions ([Fig. 7a](#)). However this modelling has a major flaw – most samples in this study were intruded into LILE- and Th-poor granulite-facies gneisses of the Assynt terrane (a geochemical feature common to deep continental crustal material – [Rudnick and Fountain \(1995\)](#)). The granulite-facies metamorphism predates the Scourie Dyke intrusion, and there is no evidence for post-intrusion tectono-metamorphic events that could have removed the LILE and/or Th. LILE-enriched amphibolite-facies gneiss only occurs in the Rhiconich and Gruinard terranes, and therefore was not available to contaminate the dolerite dykes in the Assynt Terrane. Additionally, a mechanism of contamination followed by prolonged lateral movement of the magmas would also provide an unsatisfactory explanation, as the same problem of the availability of a suitable contaminant would apply. Furthermore, there is no systematic change in composition of the Scourie Dykes across the basement terrane boundaries, indicating that local crustal contamination could not have been a major factor. Therefore this model is inappropriate for most Scourie dolerite dykes.

Assimilation of Lewisian granulite TTG ([Rollinson, 2012](#)) in AFC models cannot fully reproduce the dolerite trace element geochemistry, with a particularly poor correlation for Th ([Fig. 7c](#)). Varying the degree of fractional crystallisation of pyroxenes and plagioclase, in addition to olivine, can explain slight nuances in individual dyke geochemistry, especially for Eu, but cannot reproduce the main geochemical features. It is noted however, that the modelled Zr and Hf concentrations can be elevated by contamination of a mantle magma with a partial melt of any Lewisian TTG composition (granulite or amphibolite), although this is insensitive to changes in melting or contamination parameters and does not account for the other trace element features of the dolerites. Principally, where did the enrichment in Th and LILE present in the dykes, but absent in Lewisian granulite-facies gneisses, come from (see [Section 7.5](#))?

#### 7.2.2. Picrite and olivine gabbro dykes

The presence of garnet is suggested by high  $[\text{Gd}/\text{Yb}]_{\text{N}}$  ratios of the olivine gabbros and picrite dykes, but trace element modelling of partial melting of a garnet lherzolite enriched mantle (EM1) source and olivine fractionation could not reproduce the normalised multi-element pattern for these two dyke sets. Furthermore, fractionation of additional mineral phases could not reproduce the Th, Nb-Ta-Ti, and LREE systematics of the picrite suite. As with dolerite dyke modelling, this implies involvement of a contaminant or a significantly modified mantle source. Although attempts to model an AFC scenario similar to that for the dolerite dykes can reproduce the trace element fingerprint of the picrite dykes, this requires contamination by Lewisian amphibolite-facies gneiss which would similarly have been unavailable in the granulite facies Assynt Terrane. An AFC model involving this material is thus unfeasible. Attempts to model the picrite and olivine gabbro dyke compositions by re-melting the residue from previous dolerite dyke magma extraction similarly failed.

Having discounted the likelihood of crustal contamination of asthenospherically-derived magmas for the Scourie Dykes, we must further consider evidence for significant addition of SCLM to their parental magmas, or the possibility of a parental magma source within the SCLM.

Although major element, mineralogical and isotopic analyses of the SCLM below the North Atlantic Craton in Greenland exist ([Bernstein et al., 1998](#); [Hanghoj et al., 2001](#); [Bizzarro and Stevenson, 2003](#); [Griffin et al., 2003, 2008](#); [Wittig et al., 2008](#); [Sand et al., 2009](#); [Wittig et al., 2010](#); [Tappe et al., 2011](#)), estimates of its trace element composition are not currently available. Therefore whole-rock geochemical analyses of spinel lherzolites from Loch Roag offer the best approximation of the sub-Lewisian SCLM. These xenoliths have been entrained in a much younger (Eocene) dyke, but nonetheless there is good evidence that once formed, lithospheric keels of

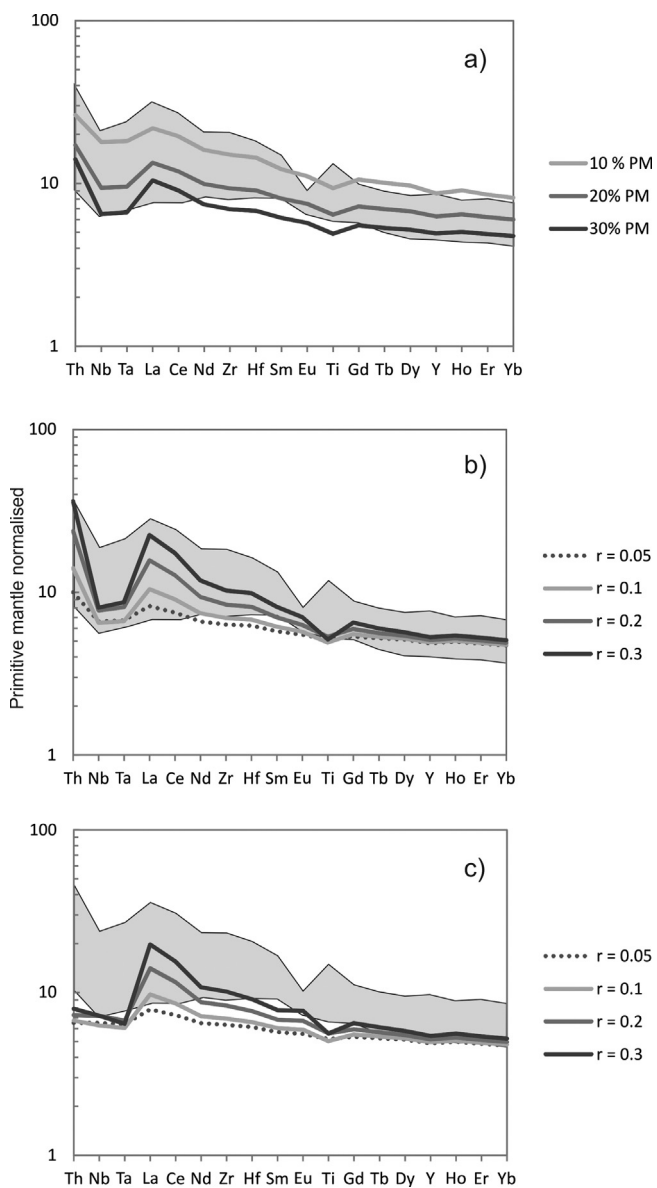


**Fig. 7.** Trace element AFC modelling for primary mantle melts with Lewisian contamination. (a) 10–30% partial melting of a spinel lherzolite primitive mantle (PM) source with assimilation ( $r=0.10$ ) of Lewisian amphibolite and fractional crystallisation fixed at 47.5% olivine. (b) 30% partial melting of a spinel lherzolite PM source with fixed fractional crystallisation of 47.5% olivine, and varying Lewisian amphibolite assimilation rates ( $r=0.05–0.30$ ). (c) Same as (b) but with assimilation of Lewisian granulite TTG. Lewisian contaminants based on Rollinson (2012).

Archaean cratons remain both physically stable and directly associated with their overlying ancient crust (O'Reilly et al., 2001; Griffin et al., 2003, 2008; Begg et al., 2010). The Lewisian Gneiss Complex has remained relatively unaffected by magmatic events since the Palaeoproterozoic (Long et al., 1991; Upton et al., 2011). Therefore for the purposes of this investigation, fresh xenolith LR80 is taken as the best available model composition for the SCLM below NW Scotland at the time of Scourie Dyke emplacement.

Modelling results indicate that, by mixing of a small degree asthenospheric partial melt (referred to here as a 'catalyst melt') with a volumetrically larger lithospheric partial melt (derived from xenolith LR80), magmas with the compositions of the various Scourie Dyke groups can be replicated. A catalyst melt representing 2–5% melting of spinel lherzolite depleted mantle (DMM), mixed with a 15% partial melt of LR80 can reproduce the trace element and general geochemical features of the dolerites (Fig. 8a and b).

Furthermore, a 10% garnet lherzolite DMM catalyst melt mixed with a 30% LR80 melt reproduces the composition of the picrite dykes (Fig. 8c and d). By varying the amount of garnet and spinel in the catalyst melt, and the fraction of the melt derived from LR80 added to the mix ( $x$ ), the trace element variability of the entire Scourie Dyke Suite can be replicated.

### 7.3. Degree of partial melting and crystal fractionation – chalcophile element evidence

The picrite and olivine gabbro dyke suites have relatively unfractionated PGE spectra. However, although the dolerite dykes show significant IPGE depletion (Fig. 5f), there is no systematic variation in PPGE concentration between the three dyke suites. Partial melting of the asthenospheric mantle initially increases Pd/Ir ratio of the melt (Keays, 1982; Barnes et al., 1988; Barnes, 1990; McDonald et al., 1995; Maier and Barnes, 2004). This is because mantle IPGE (including Ir) are mainly hosted by an Fe-rich monosulphide solid solution (MSS) often included in silicate minerals, and/or as refractory metal alloys (Os-Ir-Ru-Rh-Pt) (Brenan and Andrews, 2001; Ahmed and Arai, 2002; Sattari et al., 2002; Bockrath et al., 2004b). In contrast, Pd is predominantly hosted by interstitial Cu-rich sulphides (Sattari et al., 2002; Bockrath et al., 2004a). Under anhydrous melting conditions, refractory MSS and metal alloys (and Ir) are retained in the residue, while Pd is gradually removed with the Cu-sulphide melt. With increasing degrees of partial melting, the Pd/Ir ratio of partial melts increases until mantle sulphides become exhausted in the source region while Ir-bearing alloys are retained. At 15–20% partial melting of fertile mantle, magmas are most fractionated with the highest Pd/Ir ratios (Naldrett, 2011). If partial melting exceeds this point, Ir-bearing alloys enter the melt, progressively lowering the Pd/Ir ratio of the magma as melting proceeds.

Assuming an initial mantle concentration of approximately 250 ppm sulphur (McDonough and Sun, 1995; Bockrath et al., 2004a) and a columnar melting regime, 15–20% partial mantle melting would almost exhaust Cu-rich sulphides, providing positively fractionated PGE spectra and Pd/Ir and Cu/Pd ratios significantly higher than mantle values. This signature can be identified in the dolerite dyke suite, but the olivine gabbros and picrites do not have such elevated Pd/Ir ratios, and overall their PGE patterns are relatively unfractionated. This implies that parental melts of the picrite and olivine gabbro dykes were generated through significantly higher degrees of mantle melting, exceeding the point of solely PPGE-bearing sulphide extraction and melting IPGE-rich phases, entraining these into the magma.

Similarly low Pd/Ir ratios might also be observed in cases of second-stage melting of a depleted or refertilised mantle source. In such environments, sulphur and Pd-bearing sulphides would have already been partially extracted, and a second melting event would effectively short-cut this process, producing comparatively IPGE-rich magmas (Keays, 1995; McDonald et al., 1995; McDonald and Viljoen, 2006). For the Scourie Dyke picrite and olivine gabbro suites however, other trace element evidence cannot be reconciled with this two-stage melting scenario, with models particularly unable to recreate the HREE fractionation so characteristic of these dyke suites.

Pd/Ir ratios of some intra-craton magmas can be lower than off-craton magmas, as exemplified by comparison of on- and off-craton kimberlites (McDonald et al., 1995). On-craton kimberlites are IPGE-rich, however this is not due to any particular Ir-rich melting process, but instead a physical entrainment of xenolithic SCLM material (including IPGE-alloy inclusions in chromite, and olivine and other silicates) during ascent. Previous work has implied that Pt/Pd ratios might be utilised to infer a metasomatic and 'on-craton' signature in magmas (Maier and Barnes, 2004) with an increased

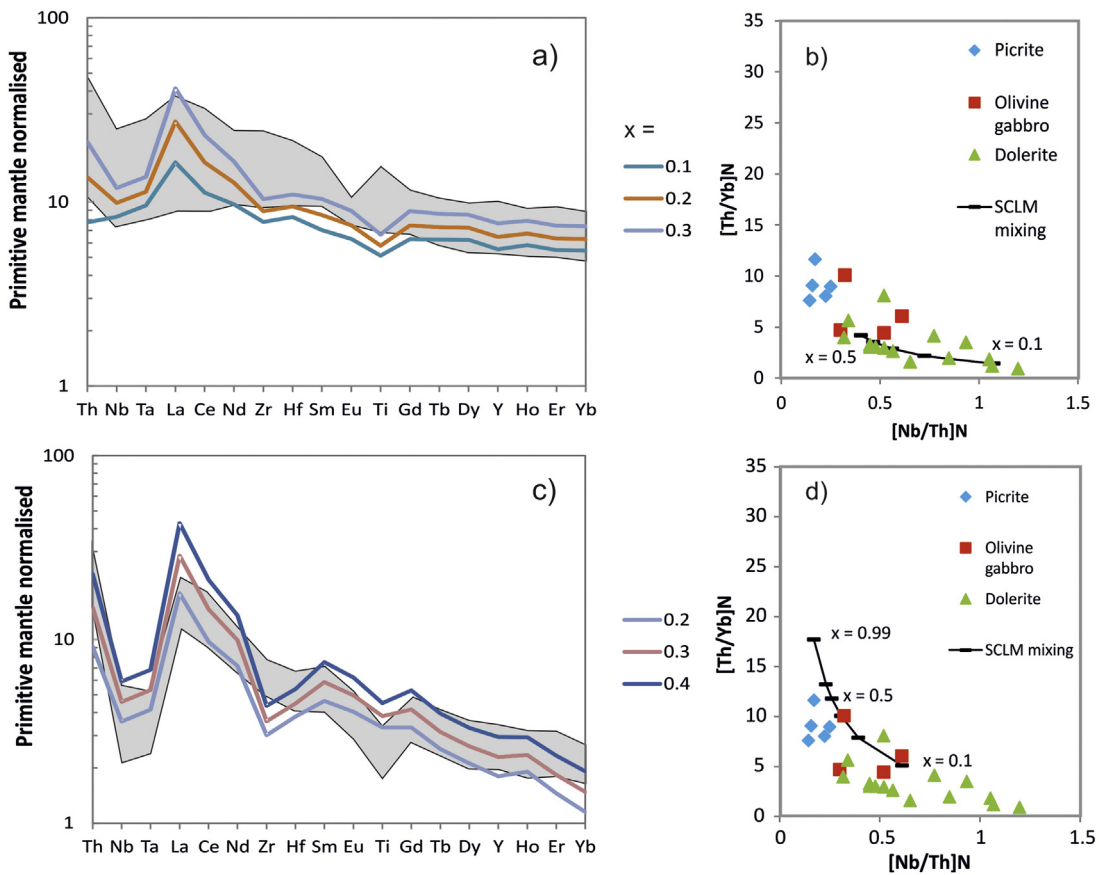


**Fig. 8.** Trace element modelling for binary mixing between primary asthenospheric mantle melts (DMM) and SCLM partial melts (using LR80 starting composition). (a) Modelling for dolerite dykes: 2–5% partial melting of a spinel lherzolite depleted mantle (DMM) source mixing with a 15% SCLM partial melt ( $x=0.10\text{--}0.30$ ). No subsequent crystal fractionation used in model. (b) Th/Yb vs Nb/Th bivariant plot for (a). (c) Modelling for picrite dykes: 10% partial melt of a DMM garnet lherzolite mixed with a 30% SCLM partial melt of LR80 ( $x=0.20\text{--}0.40$ ). (d) Th/Yb vs Nb/Th bivariant plot for (c).

Pt/Pd ratio limited to metasomatic fluid-alteration effects. However, this does not reflect the physical nature of entrainment originally proposed for kimberlites (McDonald et al., 1995), and can readily be tested by plotting Pt/Pd against another metasomatic indicator, Nb/La for example. No correlation exists between Pt/Pd and Nb/La ratios for the Scourie Dyke Suite, suggesting that the Pt/Pd ratio is insensitive to SCLM magma input or changes in SCLM geochemistry. However, the range of Pt/Pd in the Scourie Dykes is comparable to that in komatiites and continental flood basalts (Maier and Barnes, 2004).

Although it cannot be entirely discounted that the relatively high IPGE content of the picrite and olivine gabbro dyke suites could arise from physical entrainment of SCLM material, mineralogical and textural evidence does not support this, as no xenolithic material occurs in these dykes. Instead, geochemical evidence such as high MgO contents and raw PGE concentrations supports the interpretation that these are high MgO magmas, produced by higher degrees (>25–30%) of partial mantle melting than the dolerites.

Finer points may also be noted from the PGE geochemistry of the Scourie Dyke Suite. Slight positive anomalies for Rh concentrations of the picrite dyke suite (Fig. 5a) are potentially indicative of Cr-spinel accumulation in these dykes, as supported by significantly higher proportions of chromite of this suite. Olivine fractionation has apparently had very little or no effect on the PGE geochemistry of both the picrite and olivine gabbro suites, suggesting that no significant olivine fractionation took place in the parental magmas of these dykes prior to emplacement, highlighting the primitive nature of these dyke suites.

#### 7.4. Summary of mantle sources, melting and modelling

From the models presented in Section 7.2, we propose that the Scourie parental magmas are derived from both the asthenosphere and lithosphere, but predominantly it was the lithospheric mantle melting that contributed most of the melt and the observed trace element signature that we observe. In other words, 30% partial melting of LR80 modelled in Fig. 8b for the picrite suite, resulted in the extraction of almost all of the sulphide component, and with it the PPGE, along with a significant proportion of the IPGE budget.

In summary, simple partial melting of asthenospheric mantle sources (i.e. PM and EM1) cannot reproduce the ‘continental-like signature’ of the Scourie Dykes. Some subtleties of the trace element signatures, particularly for dolerites, can be accounted for by inferring some degree of crustal contamination, but by components not available to the magma at the observed level of intrusion. Moreover this contamination signature is highly variable and a very minor feature of very particular trace element abundances (Zr-Hf) in the dykes. Models highlight the insensitivity of Zr and Hf abundances during AFC or any mechanism of crustal contamination, and any ‘crustal’ signature is easily out-weighed by the strong component of lithospheric mantle.

Comparison of whole-rock geochemistry of the Scourie Dykes to that of spinel lherzolite xenoliths of Loch Roag can account for many significant similarities (e.g., Nb-Ta-(Ti) negative anomalies, and positive anomalies for Th, LILE and LREE). SCLM compositions underlying Archaean cratons are extremely variable. However the position of the Loch Roag xenoliths within the

undisturbed Lewisian Gneiss Complex at the margin of the fragmented NAC provides a rare and valuable insight into the ancient shallow mantle composition and its potential to produce later melts.

The hypothesis that all parental magmas of the Scourie Dyke Suite involved melting of enriched and modified SCLM, with a trigger input from asthenospherically derived melts, is supported by the Re-Os isotope data (Frick, 1998; this study). The  $\gamma\text{Os}_{(\text{initial})}$  values for the picrites<sup>1</sup> (−1.89 to 4.30; Frick, 1998; −6.84 for X23, this study) indicate significant and prolonged isolation of the magma source from a convecting asthenospheric source, suggesting that the Scourie Dyke magmas were lithospheric. The  $^{187}\text{Os}/^{188}\text{Os}_{(\text{initial})}$  obtained for picrite dyke (sample X23) is 0.10. In comparison the  $\gamma\text{Os}_{(\text{initial})}$  value of an earlier dolerite dyke is 2470, significantly more radiogenic than the later picrite values, and could suggest no prolonged isolation had occurred in the parental magma source of the dolerites (Frick, 1998). An  $^{187}\text{Os}/^{188}\text{Os}_{(\text{initial})}$  of 9.73 was obtained for the centre of the 'Graveyard' dolerite dyke (this study) but we suggest that the high Re content of the dyke indicates resetting of the isotopic system for this sample. New Re-Os analyses of the xenolith LR80 yields  $^{187}\text{Os}/^{188}\text{Os}_{(\text{initial})} = 0.127$  (using 45.2 Ma age; Faithfull et al., 2012)) or 0.07 (using 2400 Ma age of dykes). At 2400 Ma or 45.2 Ma, the  $^{187}\text{Os}/^{188}\text{Os}_{(\text{initial})}$  is too unradiogenic for the calculated mantle ranges at those times (0.11–0.5 at 2400 Ma, 0.128 at 45.2 Ma). This suggests isolation from the convecting mantle by 2400 Ma, but there may also be some disturbance of the isotopic system.

Sm-Nd and U-Pb isotopic analyses of the dykes in Waters et al. (1990) have a considerable range of initial compositions which indicated a component of old and enriched lithosphere. Waters and co-authors propose that a complex mixing between depleted mantle melts and enriched mantle lithosphere, isolated from the convecting asthenosphere, could have caused and dominated the combined isotope systematics of the Scourie Dykes.

The trigger for lithospheric melting might have been the thermal anomaly associated with an impinging mantle plume. However, continental extension alone could be sufficient to initiate a significant degree of partial melting both in the asthenosphere and in the fluid-rich metasomatised SCLM. Extension of the continental lithosphere generates little melt unless  $\beta$  (amount of crustal stretching) > 2 and  $T_p$  (mantle potential temperature) > 1380 °C (McKenzie and Bickle, 1988) at which point melting will occur in the asthenosphere and also the hydrous lithosphere (Gallagher and Hawkesworth, 1992). Based on field evidence, it is reasonable to suggest that a very significant degree of stretching took place during the emplacement of the Scourie Dyke swarm ( $\beta > 2$ ). In addition, numerous models (Richer, 1988; Korenaga, 2008; Davies, 2009; Herzberg et al., 2010) indicate that the mantle temperature in the Late Archaean/Palaeoproterozoic exceeded 1380 °C. Once  $\beta > 2$ , alkali basalts are produced by decompression melting, and as the degree of melting increases, tholeiites are produced.

Gd/Yb ratios and HREE spectra indicate a significantly different magma source for picrites and olivine gabbro dykes relative to the more abundant dolerite dyke suite – dolerites were derived from a source producing a flat HREE signature but olivine gabbro and picrite suites stem from a source producing a HREE-depleted signature. This is not explicable by only a change in the degree of partial melting, or by subsequent crystal fractionation. If the Scourie Dykes display a predominantly SCLM geochemical signature, then a change in the degree and depth or loci of melting, and proportions of magma inputs from the lithospheric and asthenospheric mantle, could cause the change in geochemical signature apparent between

dyke groups. However we hesitate to suggest that any garnet-bearing signature in this environment would truly be at the garnet stability depth. Instead it is likely that a lithospheric source might have undergone numerous melting/freezing magmatic events, and hence a garnet-like signature could have migrated from deeper levels and solidified in shallower lithospheric zones, resulting in an inherent heterogeneity of the Scottish lithosphere. These frozen melts could have subsequently been remobilised by the Scourie magmatic event (Fig. 9). This is supported by whole-rock geochemical evidence from the Loch Roag spinel lherzolite xenoliths. The NW Scottish SCLM's apparent heterogeneity may be due to the variable penetration of fluids, volatiles and low-degree partial melts (e.g., carbonatite or alkaline) (Fig. 9). Whether through a subduction process, or via some other metasomatic mechanism (Section 7.5), this resulted in alteration, thickening, and continued preservation of the Lewisian mantle keel (Rollinson, 2012).

### 7.5. Th-Nb-Ta-Ti and Zr-Hf anomalies – a relict Archaean subduction or metasomatic signature?

Significant negative Nb-Ta-(Ti) anomalies can be identified on the primitive mantle-normalised multi-element diagrams (Figs. 3 and 6), particularly in the picrite dykes and Loch Roag xenoliths. Modelling (Section 7.4) has shown that it is unlikely to be due to crustal contamination and may represent variation in the parental magma source. While the Scourie Dykes themselves were formed during the early Palaeoproterozoic, their lithospheric mantle source regions would have an older enrichment signature. Thus, this geochemical signature could likely be traced back into the Archaean. When seen in younger Palaeozoic to Cenozoic-age rocks, this geochemistry can be characteristic of subduction-related volcanic arc rocks. Modern basalt geochemistry can be used to infer differing tectonic environments (Hofmann, 1997; Pearce, 2008) and consistent chemical behaviour of element groups supports the idea that this can be extended to Archaean rocks (Polat and Kerrich, 2006). However controversy still surrounds the interpretation and implications of this in Archaean-Palaeoproterozoic rocks (Jenner et al., 2013) although sanukitoid occurrences across the Archaean-Proterozoic transition may mark a transition from TTG-dominated granitoid magmatism to modern-style arc magmatism (Martin et al., 2010).

Evidence for the inheritance of an Archaean metasomatised signature (rather than crustal contamination) is particularly supported by the enrichment of Th and LILE in the dyke suite relative to the Th- and LILE-depleted Lewisian granulite-facies TTG. All members of the Scourie Dyke Suite sampled during this study (regardless of terrane – see Section 7.1) have much higher concentrations of these elements. This implies that combined LILE and Th enrichment is a key feature of the mantle that produced the Scourie Dykes, i.e., akin to the Loch Roag xenoliths. These features are suggestive of upper mantle alteration and enrichment via a metasomatic mechanism (Hawkesworth et al., 1994; Pearce et al., 2005). But the negative Zr-Hf anomaly observed in Loch Roag in particular indicates a carbonate/carbonatite-metasomatic event, rather than solely a silicate alkali or volatile-only event (Yaxley et al., 1991, 1998; Ionov and Harmer, 2002; Pearson et al., 2003). This may have been related to subduction in the Archaean, which is possibly suggested by  $\delta^{18}\text{O}$  data for the dykes (Davies et al., 2012) and previously published whole-rock and mineral  $\delta^{18}\text{O}$  (Cartwright and Valley, 1991). Cartwright and Valley (1991) demonstrated that the low- $\delta^{18}\text{O}$  magmas of the Scourie Dykes were unlikely to have been caused by the assimilation of large volumes of continental crust, and this signature was more probably derived from a low- $\delta^{18}\text{O}$  subduction-modified lithospheric mantle source.

Modification of the sub-Lewisian shallow mantle took place prior to xenolith entrainment, but the timing of this event is

<sup>1</sup>  $\gamma\text{Os}_{(\text{initial})}$  calculated at an emplacement age of 2400 Ma and 2000 Ma for the picrite and dolerite dykes, respectively (Frick, 1998). See Appendix C.

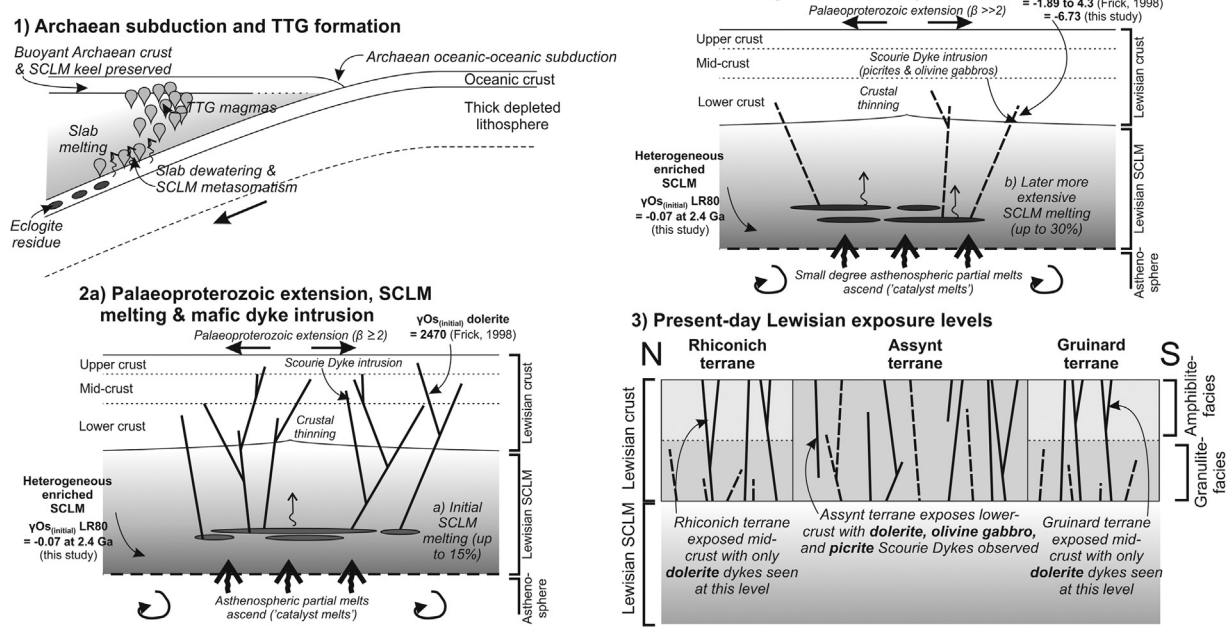


**Fig. 9.** Model scenario for formation of Lewisian depth-zoned SCLM and Scourie Dyke Suites. (1) Archaean subduction during Lewisian TTG formation (based on Rollinson (2010)) – subduction of dense Fe-rich oceanic crust and thick depleted lithosphere, causing slab dewatering and melting and over-riding mantle wedge (SCLM) metasomatism. Slab melts (TTG magma precursors) eventually form buoyant Archaean crust and preserved buoyant SCLM. (2a) Palaeoproterozoic extension causes decompression melting in asthenosphere and subduction-enriched SCLM producing dolerite dyke parental magmas. This is followed by (2b) higher degree partial melting of subduction-enriched SCLM producing parental magmas of the olivine gabbro dykes and picrite dykes. Magmas ascend and are emplaced into Lewisian crust, although denser Mg-rich olivine gabbro and picrite dyke magmas only penetrate lower crustal levels.  $\gamma\text{Os}_{\text{initial}}$  values from Frick (1998) and this study. (3) Later tectonic displacement and erosion to present-day exposure levels see the Rhiconich and Gruinard Terranes with mid-crustal amphibolite-facies Lewisian gneiss and only the dolerite dyke suite encountered. In contrast, the Assynt Terrane is a lower crust granulite-facies block with all three dyke suites exposed. See text for discussion.

uncertain. Time-integrated Nd isotopic ratios of the Loch Roag peridotite xenoliths and associated xenocrysts have suggested two or more periods of lithospheric mantle metasomatism – one at 1.0–1.5 Ga (Menzies et al., 1987), and one at 2.3–2.5 Ga (Long et al., 1991). On this basis, at least some upper mantle metasomatism and enrichment was already underway by the time of Scourie Dyke magmatism. Long et al. (1991) suggest that carbonatite-based metasomatism was prevalent during the 2.3–2.5 Ga event. If this is the case, this age overlaps with that of the age of the Scourie Dykes, and may be a deeper indication of continental rifting. Alternatively, a similar metasomatic signature might have occurred in addition to, or prior to extension, via an older subduction process recorded in the lithospheric mantle – a ‘relic’ Archaean subduction signature preserved in Archaean SCLM, and incorporated into dyke magmas during Palaeoproterozoic extension.

The protoliths to the Lewisian TTG gneisses are 3.0–2.7 Ga (Kinny et al., 2005). Recent work on the Re-Os isotopic composition of peridotite xenoliths from the NAC in W Greenland has discovered significant metasomatic enrichment and melt extraction at 2.0 Ga, but other xenoliths from a similar area have model Re depletion ages of 2.7–3.1 Ga (Wittig et al., 2010). Overall these xenoliths record lithospheric stabilisation between the Meso- to Neoarchaean, followed by metasomatic alteration and overprinting magmatic events. In particular, the FeO enrichment of some of the W Greenland peridotites (comparable to the Fe enrichment observed in the Loch Roag xenoliths), and HREE abundances, are thought to require SCLM depletion in a relatively shallow subduction zone and/or mid-ocean ridge setting (Wittig et al., 2010).

Overall, if a mid-late Archaean slab subduction regime is accepted (Rollinson, 2010), it has implications for Archaean mantle and cratonic SCLM geochemistry. We may expect an enrichment of LILE and LREE, and mobilisation of sulphur through mantle wedge metasomatism and hydrous partial melting. Thus the SCLM keels

of Archaean cratons may host complex and heterogeneous hydrous subduction-modified geochemical signatures. Indeed, we find that direct samples of the SCLM below NW Scotland share these geochemical facets. This complexity would only be expected to be preserved in the lithospheric mantle (and likely in a heterogeneous manner), with convecting asthenosphere not retaining the subduction/metamorphic signature. As previously discussed in Sections 7.2–7.4, the metasomatised complexities of the Lewisian lithospheric mantle keel are vital for understanding the trace element characteristics of the Scourie Dyke Swarm.

#### 7.6. Lewisian SCLM geochemistry: evidence of melting mechanism – plume or no plume?

With the acceptance of an ancient subduction signature being present in the Palaeoproterozoic Scourie Dyke Swarm, the intricacies of this scenario and the melting mechanism may be scrutinised further. LREE concentrations of the Scourie Dyke suites are very enriched (Fig. 3), comparable to some alkaline magmas globally (e.g., McDonald et al., 1995), especially taking into consideration the high degrees of partial melting indicated for the ultramafic magmas by the IPGE data. This further highlights the substantial LREE metasomatic enrichment of the mantle source. Multi-element plots (e.g., Fig. 6a) of each of the dyke suites show a comparable, but progressively exaggerated ‘metasomatic’ signature, which becomes increasingly more discernible from the dolerites through to the olivine gabbro and picrite suites (i.e., from mafic to ultramafic compositions). This presents a paradox for any melting model incorporating a plume (with contamination).

Asthenospheric melts producing progressively increasing degrees of melting should dilute any initial geochemical anomaly such as that for Nb-Ta-Ti. In addition the relative ages of the dolerite (mafic) and picrite (ultramafic) dyke groups may provide clues

as to the presence of a plume. Recent geochronological work has highlighted the long time-period over which Scourie dykes were intruded (400 Myr) (Davies and Heaman, 2014) but the majority were apparently intruded over a shorter 'main' period spanning ~40 Myr between 2418 and 2375 Ma (Davies and Heaman, 2014) which itself has apparent temporal subdivisions. Overall, this prolonged phase of dyke intrusion is exceptional for any Large Igneous Province (LIP) globally (flood basalt-related events are observed to last ~1–5 Myr, Ernst et al., 2013), but in Scourie these appear to have been intruded in 'pulses' over at least 40 Myr. The uniformity of dyke azimuth and longevity of intrusion dates could instead be the result of persistent rifting, as observed in the Tarim block of NW China (Zhu et al., 2008; Davies and Heaman, 2014).

## 8. Conclusions

1. Geochemical modelling of the Scourie Dyke Swarm has shown that the swarm could not have been derived from an asthenospheric mantle region with variable crustal contamination using the available crustal components. Therefore we investigate where such an enriched geochemical signature could have been sourced.
2. Negative Nb-Ta-Ti anomalies, and enrichments in Th, LREE and other LILE, particularly in the picrite suite represent an Archaean metasomatic geochemical signature in the lithospheric mantle. This could indicate that a shallow-angle subduction regime was present during formation of the Lewisian portion of the North Atlantic Craton, and/or that carbonatite-induced metasomatism was coeval with the rifting event that led to the intrusion of the Scourie Dykes themselves.
3. Whole-rock geochemical analyses, and a new measurement of the Re-Os isotopic composition of spinel lherzolite mantle xenoliths from Loch Roag confirm the presence of this signature in the shallow mantle underlying this region of Scotland, and corroborate the presence of significant metasomatic enrichment of the mantle lithospheric keel of the Lewisian portion of the NAC.
4. Despite Loch Roag xenolith chemical continuity, the Archaean sub-Lewisian SCLM is likely to be heterogeneous, due to varying degrees of metasomatism and partial melting throughout Lewisian TTG and SCLM keel formation.
5. Dolerite and picrite dykes were derived from different parts of the heterogeneous lithosphere, with variable HREE signatures. However, using HREE to make interpretations of the depth of melting within the heterogeneous SCLM is inappropriate due to the possibility of 'frozen-in' signatures imparted during prolonged formation and alteration.
6. PGE can be used to further characterise mantle melting regimes and the extent of partial melting. Ir-group PGE depletion in dolerite dykes suggests up to 15% partial melting of the SCLM source, while low Pd/Ir ratios in both the picrite and olivine gabbro dyke suites highlight a significantly higher degree of melting (>25–30%) within a fluid-rich lithospheric mantle source.
7. Our trace element geochemical modelling suggests that the Scourie Dykes have variably sampled this enriched and fusible lithospheric mantle region through direct partial melting of the metasomatised SCLM itself, possibly coupled with, or triggered by, some degree of asthenospheric melting. This was a direct result of tectonic extension causing lithospheric thinning and decompression.

## Acknowledgements

HSRH would like to acknowledge the financial support of the Natural Environment Research Council (NERC) for funding this work which has been undertaken as part of her PhD (studentship NE/J50029X/1). Hilary Downes and Hugh Rollinson are thanked for their thorough and detailed review of the manuscript, and Randy Parrish is thanked for his constructive comments. HSRH and co-authors wish to thank Scottish Natural Heritage (SNH) and numerous landowners for their kind permission to sample the Scourie Dykes. Lawrence Badham is thanked for his assistance in making polished thin sections for study. KMG publishes with the permission of the Executive Director of the British Geological Survey. Discussions with Julian Pearce and Nicholas Arndt were much appreciated during the writing of this manuscript.

## Appendix A.

Table of all dyke results used throughout paper, in addition to Table 1.

Sample	X6 D.c NC 1415 4418	X7 D.m NC 1477 4485	X8 D.c NC 1473 4488	X9 D.m NC 1480 4485	X10 OG.c NC 1548 4474	X12 D.c NC 1637 4872	X13 D.c NC 1645 4866	X15 D.c NC 1726 4975	X17 D.m NC 1889 4531	X18 D.c NC 1889 4531
Grid ref.	(wt.%)									
SiO <sub>2</sub>	50.92	46.38	43.43	46.84	47.64	48.55	47.09	51.22	49.97	49.97
TiO <sub>2</sub>	2.63	3.22	3.14	3.25	1.41	2.25	2.81	1.66	2.01	1.66
Al <sub>2</sub> O <sub>3</sub>	12.42	12.61	12.12	12.58	7.26	10.57	10.56	12.89	12.59	13.51
Fe <sub>2</sub> O <sub>3</sub> *	17.72	20.55	21.21	19.19	14.54	20.00	21.37	15.71	16.33	15.65
MnO	0.27	0.29	0.28	0.27	0.22	0.35	0.29	0.23	0.24	0.25
MgO	4.49	5.02	5.85	4.85	16.51	6.07	5.32	5.63	5.74	6.21
CaO	8.67	9.50	10.01	9.16	9.08	8.41	7.95	8.52	8.94	9.91
Na <sub>2</sub> O	2.26	2.57	2.43	2.61	1.56	2.02	2.20	2.78	2.26	2.40
K <sub>2</sub> O	1.15	0.55	0.40	0.57	0.12	0.77	0.73	1.09	0.85	0.82
P <sub>2</sub> O <sub>5</sub>	0.35	0.26	0.22	0.36	0.12	0.24	0.21	0.16	0.21	0.16
LOI	0.13	0.33	0.31	1.28	0.62	1.00	1.38	1.23	1.30	0.64
Total	101.01	101.28	99.41	100.97	99.09	100.23	99.92	101.12	100.44	101.18
(ppm)										
Sc	44	42	50	44	28	50	48	42	41	45
V	456	582	566	450	255	559	539	416	383	375
Cr	246	32	33	30	1689	106	110	108	124	146
Co	48	60	59	53	129	59	51	49	55	55
Ni	104	73	70	77	1213	115	68	79	86	123
Cu	108	92	88	90	139	57	94	110	242	173
Rb	28	11	10	12	1	25	20	28	16	12
Sr	150	174	149	186	135	169	92	160	142	204
Y	61	35	35	47	15	45	41	35	38	31
Zr	265	124	115	123	80	151	170	141	168	110
Nb	13.2	8.4	7.6	14.1	6.3	11.7	10.5	6.3	11.0	7.5
Ba	332	140	123	178	73	190	148	185	163	149
La	25.02	10.01	9.23	13.59	9.34	11.76	6.50	11.75	14.08	10.03
Ce	61.15	24.42	22.63	33.67	23.66	27.77	17.92	28.18	32.81	23.72
Pr	8.25	3.79	3.58	5.30	3.64	4.44	2.84	4.22	4.91	3.60
Nd	34.06	17.12	16.16	23.77	15.40	19.80	13.62	18.01	21.06	15.49
Sm	8.33	4.63	4.62	6.46	3.74	5.39	4.44	4.57	5.49	4.20
Eu	2.13	1.61	1.52	1.85	1.08	1.68	1.41	1.36	1.57	1.22
Gd	7.99	4.87	4.72	6.03	3.21	5.73	4.71	4.67	5.15	4.00
Tb	1.36	0.85	0.87	1.06	0.51	1.04	0.90	0.82	0.93	0.75
Dy	8.75	5.53	5.54	6.75	2.79	6.79	6.15	5.30	5.93	4.73
Ho	1.81	1.17	1.14	1.40	0.52	1.42	1.28	1.11	1.24	0.97
Er	5.31	3.30	3.38	4.04	1.41	4.29	3.81	3.22	3.65	2.89
Tm	0.76	0.48	0.49	0.57	0.19	0.61	0.55	0.48	0.52	0.43
Yb	4.98	3.18	3.08	3.80	1.15	4.08	3.82	3.10	3.59	2.92
Lu	0.79	0.50	0.50	0.60	0.17	0.66	0.61	0.49	0.54	0.45
Hf	6.95	3.09	3.10	3.13	2.40	4.02	3.80	3.65	4.00	2.91
Ta	0.73	0.53	0.41	1.06	0.46	1.05	0.62	0.45	0.82	0.46
Th	3.57	1.30	1.09	1.22	1.25	1.34	1.43	1.92	1.46	1.09
U	0.94	0.28	0.26	0.30	0.31	1.25	0.53	0.53	0.41	0.28

X20 D.c NC 1679 4427	X21 D.m NC 1679 4427	X22 P.c NC 1449 2255	X23 P.c NC 1447 2256	X24 D.c NC 1462 2282	X25 P.c NC 1451 2283	X26 P.c NC 1448 2283	X27 P.m NC 1487 2395	X28 D.c NC 1698 2581	X29 D.m NC 1717 2602	X30 D.c NC 1717 2602	X31 D.c NC 1717 2602
49.73	50.73	48.27	49.63	51.00	47.43	50.25	52.50	51.12	49.83	50.48	51.07
1.16	0.81	0.47	0.67	0.31	0.47	0.36	0.68	0.71	1.69	1.30	1.63
14.96	14.55	6.46	10.61	5.11	7.23	6.19	7.39	15.13	12.91	13.27	12.86
11.47	12.62	12.06	11.21	11.91	11.10	11.07	12.23	10.17	16.76	15.90	17.19
0.21	0.20	0.17	0.16	0.17	0.15	0.17	0.19	0.18	0.25	0.23	0.27
7.47	6.56	22.15	17.36	23.10	19.81	21.52	16.34	6.37	5.04	5.80	4.89
9.43	10.21	4.92	6.37	4.65	5.16	5.64	7.32	10.60	7.89	9.96	8.23
2.46	2.32	1.32	2.22	0.27	0.47	1.22	1.37	3.07	2.60	2.55	3.00
0.54	0.74	0.53	0.69	0.01	1.03	0.46	0.76	0.65	0.42	0.36	0.66
0.10	0.06	0.06	0.11	0.03	0.07	0.05	0.10	0.07	0.17	0.12	0.18
2.96	1.54	2.82	2.06	3.39	6.88	2.54	1.18	0.99	1.77	0.69	0.77
100.47	100.32	99.23	101.09	99.96	99.80	99.46	100.04	99.06	99.30	100.66	100.73
41	35	17	19	19	18	19	25	32	36	42	38
335	290	142	176	116	146	132	218	250	445	411	410
112	71	3134	1918	4051	3891	4432	2823	320	258	41	56
57	58	160	114	148	142	157	93	48	64	63	60
109	153	1841	1261	1712	1474	1587	909	161	84	66	99
247	146	51	112	18	167	54	42	56	239	231	164
9	11	16	22	1	31	12	22	6	4	10	15
182	216	171	258	17	109	155	78	339	173	166	218
28	19	10	14	7	10	9	15	20	36	29	37
96	63	64	73	34	70	55	81	65	108	87	153
5.9	3.5	2.5	3.1	0.9	2.9	1.6	3.7	3.5	7.4	4.5	7.8
123	189	317	366	10	174	315	239	261	108	95	159
7.81	5.23	9.78	13.87	2.16	10.78	8.43	14.02	12.92	9.42	7.54	12.00
18.73	12.39	20.22	28.58	6.54	21.75	17.27	30.45	29.31	23.13	17.51	27.41
2.81	1.90	2.64	3.76	1.15	2.84	2.23	3.97	4.08	3.57	2.65	4.04
12.56	8.27	10.10	14.11	5.11	10.30	8.42	14.65	15.72	15.59	11.72	17.66
3.66	2.34	2.09	2.80	1.16	2.00	1.68	2.88	3.29	4.32	3.34	4.83
1.11	0.79	0.58	0.80	0.29	0.62	0.52	0.75	1.13	1.45	1.06	1.52
3.50	2.32	1.73	2.41	1.07	1.83	1.54	2.62	3.10	4.59	3.33	4.74
0.66	0.45	0.27	0.38	0.17	0.27	0.24	0.42	0.51	0.87	0.63	0.87
4.24	2.90	1.67	2.15	1.06	1.60	1.37	2.44	3.15	5.69	4.12	5.67
0.88	0.60	0.33	0.42	0.21	0.31	0.27	0.48	0.64	1.15	0.85	1.15
2.64	1.80	0.93	1.20	0.60	0.91	0.81	1.38	1.85	3.45	2.55	3.44
0.38	0.26	0.13	0.18	0.09	0.13	0.11	0.20	0.27	0.51	0.38	0.48
2.49	1.84	0.87	1.15	0.57	0.88	0.75	1.23	1.84	3.47	2.54	3.38
0.37	0.27	0.13	0.17	0.09	0.13	0.11	0.19	0.28	0.52	0.38	0.51
2.82	1.63	1.57	1.66	0.83	1.85	1.18	1.89	1.53	3.28	2.42	3.79
0.37	0.20	0.15	0.21	0.07	0.21	0.09	0.19	0.22	0.49	0.27	0.49
1.29	0.82	1.45	1.66	0.80	1.42	1.22	2.58	0.39	1.55	1.06	1.79
0.89	0.20	0.26	0.35	0.11	0.28	0.21	0.60	0.12	0.39	0.26	0.35

## Appendix A (Continued)

X32 D.c NC 1717 2602	X33 D.c NC 1197 1605	X34 D.c NC 1197 1605	X35 D.c NC 1201 1606	X36 OG.c NC 1197 1690	X37 OG.c NC 0741 2105	X38 D.c NC 0746 2200	X39 D.c NC 0820 2057	X40 D.m NC 1455 4161	X41 D.c NC 1455 4161	X42 D.m NC 1455 4161	X43 D.c NC 1513 4145
51.49	50.59	50.30	50.41	47.97	45.27	51.00	47.92	51.13	50.77	51.25	48.08
1.68	1.70	1.82	1.90	1.62	1.96	1.72	1.79	1.75	1.61	2.04	1.45
14.48	12.83	12.88	12.94	11.86	8.62	13.29	12.31	13.13	13.30	13.03	14.18
15.48	15.63	16.51	16.84	14.98	19.00	17.55	18.61	15.83	15.95	16.89	14.10
0.26	0.24	0.24	0.24	0.20	0.23	0.23	0.28	0.23	0.22	0.26	0.19
4.30	5.27	5.10	5.28	11.07	13.82	4.48	6.64	5.39	5.44	4.84	7.07
7.61	9.17	8.50	9.23	7.96	8.96	6.91	7.60	8.86	8.62	8.12	11.28
3.06	2.40	2.57	2.54	3.32	2.34	2.94	3.16	2.43	2.82	2.65	2.73
0.73	0.66	0.73	0.70	0.77	0.52	1.04	0.71	0.69	1.03	0.87	0.35
0.16	0.17	0.17	0.20	0.21	0.11	0.16	0.11	0.29	0.28	0.43	0.07
0.76	0.31	0.43	0.31	0.36	0.25	1.43	1.96	0.70	0.93	0.94	1.57
100.01	98.97	99.25	100.58	100.32	101.07	100.76	101.09	100.44	100.98	101.31	101.08
31	42	40	42	25	30	37	48	37	37	36	49
406	450	388	429	304	435	396	556	341	378	438	583
24	160	126	151	910	1294	20	186	61	59	45	175
57	59	51	54	85	142	49	68	48	53	59	65
48	93	77	89	709	844	67	93	261	63	75	92
189	196	149	185	122	131	197	1055	125	223	180	212
18	19	19	21	18	12	20	15	7	15	12	6
236	173	175	166	332	200	176	132	262	219	345	175
33	41	39	43	23	20	35	31	34	34	43	24
96	174	131	188	182	109	84	93	183	184	230	54
7.9	7.9	7.8	8.6	7.7	5.0	5.8	4.4	8.3	8.7	11.2	2.7
178	227	249	255	266	175	401	168	240	500	400	92
9.67	15.15	14.42	17.03	15.93	9.79	8.50	5.34	22.67	22.87	31.99	3.91
23.35	34.16	32.67	38.35	35.62	23.22	20.99	13.83	49.13	48.76	69.33	10.36
3.58	4.95	4.83	5.65	5.12	3.53	3.27	2.31	6.85	6.84	9.96	1.77
15.59	21.07	20.53	23.54	21.81	15.76	14.65	11.13	27.50	27.53	39.83	8.35
4.23	5.27	5.60	6.07	5.63	4.19	4.37	3.62	6.34	6.33	8.90	2.83
1.44	1.49	1.49	1.56	1.50	1.19	1.36	1.10	1.60	1.48	2.13	0.87
4.27	5.42	5.24	5.81	4.59	3.63	4.33	3.74	5.36	4.68	7.10	2.78
0.77	0.96	0.92	1.03	0.73	0.61	0.81	0.72	0.86	0.74	1.07	0.52
5.09	6.10	6.19	6.67	4.12	3.50	5.47	4.86	5.19	4.48	6.48	3.55
1.04	1.28	1.25	1.34	0.76	0.64	1.09	1.02	1.04	0.90	1.25	0.71
3.06	3.80	3.72	4.03	2.04	1.75	3.28	2.92	3.06	2.70	3.76	2.17
0.43	0.57	0.54	0.58	0.26	0.23	0.46	0.43	0.43	0.38	0.53	0.32
3.06	3.87	3.58	3.92	1.59	1.44	3.09	2.84	2.89	2.50	3.53	2.12
0.45	0.59	0.59	0.64	0.27	0.23	0.53	0.49	0.47	0.42	0.58	0.35
3.54	4.15	3.60	4.82	4.45	3.31	3.16	2.49	4.49	3.86	5.13	1.38
0.56	0.44	0.37	0.44	0.49	0.28	0.30	0.27	0.44	0.43	0.55	0.18
1.22	2.12	1.96	2.31	2.90	1.15	1.52	0.82	2.93	2.36	2.90	0.41
0.26	0.52	0.56	0.60	0.37	0.24	0.57	0.25	0.67	0.57	0.78	0.09

X44 D.c NG 9866 9240	X45 D.c NG 9842 9243	X47 D.c NG 9836 9235	X50 D.c NG 9552 9044	X51 D.m NG 9552 9044	X52 OG.c NG 9602 9276	X53 D.c NC 2481 4691	X54 D.c NC 2485 4711	X55 D.c NC 2303 4821	X56 D.c NC 2303 4821	X59 D.c NC 2241 5648
50.05	51.79	51.60	51.94	49.66	48.10	50.67	51.53	47.97	49.08	52.62
1.49	1.84	2.27	1.52	1.63	1.34	1.75	1.62	2.43	3.05	1.79
9.57	13.42	12.48	12.56	13.27	10.14	13.06	12.45	14.03	13.99	12.84
14.60	15.33	16.57	14.02	14.19	13.37	14.05	15.59	16.43	16.76	15.64
0.22	0.23	0.25	0.22	0.21	0.21	0.25	0.26	0.24	0.28	0.21
10.00	5.02	4.53	6.30	6.76	12.25	5.09	5.59	5.72	4.69	4.45
9.57	8.37	7.38	11.45	9.91	9.71	8.10	10.07	8.62	6.74	8.15
2.39	2.79	2.78	1.80	2.60	2.52	3.42	2.54	2.85	3.04	2.74
0.72	0.95	1.78	0.40	0.58	0.28	1.71	1.03	1.80	2.18	1.13
0.18	0.57	0.25	0.13	0.12	0.12	0.16	0.15	0.37	0.46	0.14
1.46	0.97	1.10	0.89	0.90	1.44	1.00	0.67	0.57	0.87	0.84
100.26	101.28	100.98	101.23	99.84	99.49	99.27	101.51	101.02	101.15	100.57
24	37	35	42	50	25	38	44	36	33	31
234	345	408	444	364	297	325	349	330	313	408
837	42	36	58	106	965	24	63	366	52	15
73	47	51	57	37	69	45	54	48	42	42
323	61	34	85	90	801	55	196	109	46	40
143	149	169	314	47	90	103	75	77	52	55
19	15	73	5	10	4	61	23	75	157	34
271	375	206	141	161	199	316	252	246	257	270
32	34	48	31	28	17	31	34	50	58	26
256	200	269	96	114	93	161	134	251	310	97
16.5	7.7	11.8	5.8	5.5	2.7	12.8	8.5	12.8	21.0	5.6
322	788	518	79	148	92	302	127	533	517	346
24.38	32.02	25.98	9.10	6.67	4.43	13.71	11.02	25.31	28.37	6.77
54.09	66.45	57.19	20.77	15.47	12.79	31.58	25.12	55.43	63.15	16.49
7.67	9.45	8.07	3.12	2.42	2.13	4.52	3.72	7.86	8.81	2.63
30.69	38.60	32.09	13.26	10.62	10.54	18.82	15.95	32.07	36.24	11.58
7.16	7.94	7.83	3.95	3.13	3.43	4.82	4.41	7.91	8.98	3.39
1.62	2.18	1.91	1.06	0.94	1.04	1.27	1.15	1.98	2.27	1.17
6.26	6.63	7.23	3.76	3.04	2.93	4.12	4.15	7.21	8.48	3.42
0.96	0.97	1.21	0.67	0.62	0.51	0.72	0.74	1.23	1.40	0.63
5.53	5.36	7.49	4.39	4.15	2.97	4.45	4.96	7.67	8.82	4.07
1.06	1.01	1.48	0.91	0.89	0.56	0.93	1.02	1.56	1.77	0.86
2.99	3.17	4.50	2.74	2.67	1.49	2.76	3.03	4.62	5.17	2.47
0.41	0.44	0.63	0.39	0.41	0.20	0.40	0.44	0.67	0.75	0.37
2.62	2.91	4.24	2.63	2.74	1.27	2.69	2.95	4.48	5.09	2.48
0.41	0.49	0.69	0.43	0.44	0.18	0.42	0.46	0.70	0.79	0.38
6.12	4.65	6.75	2.95	2.86	2.71	3.71	3.15	5.61	7.34	3.00
0.85	0.54	0.55	0.33	0.35	0.21	0.71	0.48	1.00	1.69	0.28
3.81	2.36	5.23	1.24	1.10	1.08	2.00	1.17	3.14	4.51	1.43
1.27	0.55	1.55	0.34	0.23	0.18	0.70	0.24	0.77	1.98	0.33

## Appendix A (Continued)

X60 D.c NC 2231 5652	X63 D.c NC 1183 3300	X65 D.c NC 0628 3125	X67 D.c NC 0573 3084	X68 P.c NC 0498 2710	X69 D.c NC 0498 2712	X71 D.c NC 0593 2510	X72 D.c NC 0587 2491
46.09	48.35	48.96	49.02	50.46	49.38	48.01	52.05
2.24	2.46	2.07	1.31	0.43	1.77	1.18	1.14
12.76	11.95	12.06	13.09	6.21	13.23	13.43	14.05
17.88	18.04	15.76	12.69	11.55	15.26	14.70	11.37
0.25	0.27	0.22	0.20	0.19	0.23	0.22	0.18
5.49	4.94	4.37	8.75	20.38	6.64	7.08	7.82
9.63	8.18	7.61	11.33	7.07	11.10	11.21	10.34
2.79	2.54	2.42	1.52	0.76	1.69	1.80	2.45
1.47	1.22	1.22	0.91	0.00	0.78	0.42	0.59
0.12	0.35	0.22	0.10	0.05	0.14	0.08	0.13
0.67	0.91	6.40	1.61	2.07	0.66	0.93	0.77
99.40	99.22	101.30	100.54	99.18	100.89	99.07	100.88
39	41	34	42	23	41	41	37
495	420	346	310	162	353	326	340
26	52	37	367	2949	62	129	204
52	45	44	51	87	49	53	45
134	53	73	156	1209	83	129	119
47	137	219	27	66	127	119	164
24	24	34	21	1	9	3	11
234	186	196	154	12	199	169	282
26	56	44	17	10	22	24	18
89	266	236	68	53	91	68	89
5.6	12.5	12.3	6.5	1.4	8.9	3.7	11.2
203	367	404	137	1	253	115	188
8.37	24.13	24.26	8.29	7.34	9.84	3.65	12.53
18.60	54.50	51.77	19.21	15.36	23.18	9.60	26.27
2.77	7.76	7.00	2.87	2.12	3.46	1.61	3.47
11.83	31.93	28.23	12.22	8.27	14.82	7.81	13.96
3.39	8.29	6.88	3.24	2.00	3.91	2.71	3.31
1.12	2.02	1.64	0.93	0.45	1.17	0.85	0.99
3.21	7.29	5.92	2.69	1.69	3.32	2.64	3.07
0.60	1.29	1.03	0.45	0.27	0.56	0.52	0.51
3.86	8.28	6.38	2.75	1.65	3.47	3.64	3.00
0.82	1.68	1.32	0.54	0.33	0.68	0.77	0.59
2.35	5.07	3.95	1.54	0.95	1.97	2.33	1.71
0.35	0.74	0.56	0.22	0.13	0.28	0.34	0.23
2.31	4.97	3.83	1.45	0.88	1.81	2.31	1.57
0.36	0.79	0.60	0.22	0.14	0.28	0.36	0.26
2.65	6.51	5.75	1.89	1.21	2.62	1.72	2.19
0.30	0.65	0.80	0.39	0.11	0.53	0.19	0.59
1.13	3.19	5.00	0.80	1.20	1.14	0.38	1.96
0.36	0.80	1.35	0.37	0.29	0.30	0.09	0.52

Analytical Recovery (international rock standard JB1-a) for ICP-OES.

	Certified value	Measured value	Analytical recovery (AR %)
SiO <sub>2</sub>	52.16	52.90	101.42
TiO <sub>2</sub>	1.30	1.31	101.11
Al <sub>2</sub> O <sub>3</sub>	14.51	14.21	97.93
Fe <sub>2</sub> O <sub>3</sub>	9.10	9.25	101.60
MnO	0.15	0.15	99.08
MgO	7.75	7.53	97.15
CaO	9.23	8.72	94.46
Na <sub>2</sub> O	2.74	2.83	103.46
K <sub>2</sub> O	1.42	1.54	108.67
P <sub>2</sub> O <sub>5</sub>	0.25	0.26	105.72
LOI	0.78	0.78	100.00
Total	99.39	99.49	100.10
Sc	27.9	27.8	99.7
V	206.0	199.3	96.7
Cr	415.0	422.1	101.7
Co	39.5	43.6	110.3
Ni	134.0	147.0	109.7
Cu	55.0	52.3	95.0
Zn	82.0	86.2	105.2
Sr	443.0	456.5	103.1
Y	24.0	24.8	103.5
Zr	146.0	151.0	103.4
Ba	497.0	504.7	101.5

Analytical Recovery (international rock standard JB1-a) for ICP-MS.

	Certified value	Measured value	Analytical recovery (AR %)
<sup>49</sup> TiO <sub>2</sub>	1.30	1.28	98.2
<sup>51</sup> V	206.0	198.0	96.1
<sup>52</sup> Cr	415.0	410.3	98.9
<sup>55</sup> MnO	0.15	0.15	96.6
<sup>57</sup> Fe <sub>2</sub> O <sub>3</sub>	9.1	9.0	98.5
<sup>59</sup> Co	39.5	37.5	94.9
<sup>60</sup> Ni	134.0	143.2	106.9
<sup>65</sup> Cu	55.0	65.1	118.3
<sup>66</sup> Zn	82.0	81.9	99.8
<sup>71</sup> Ga	18.0	18.6	103.5
<sup>85</sup> Rb	42.0	40.1	95.6
<sup>88</sup> Sr	443.0	438.3	98.9
<sup>89</sup> Y	24.0	24.5	102.2
<sup>90</sup> Zr	146.0	144.1	98.7
<sup>93</sup> Nb	27	28.0	103.6
<sup>95</sup> Mo	1.29	1.29	100.0
<sup>118</sup> Sn	2.45	2.45	100.0
<sup>133</sup> Cs	1.2	1.3	110.3
<sup>137</sup> Ba	497.0	511.2	102.8
<sup>139</sup> La	38.1	38.8	101.9
<sup>140</sup> Ce	66.1	66.7	101.0
<sup>141</sup> Pr	7.3	7.5	103.3
<sup>146</sup> Nd	25.5	26.5	104.0
<sup>147</sup> Sm	5.02	5.14	102.5
<sup>153</sup> Eu	1.47	1.48	100.5
<sup>157</sup> Gd	4.54	4.53	99.8
<sup>159</sup> Tb	0.69	0.67	97.1
<sup>163</sup> Dy	4.19	3.84	91.7
<sup>165</sup> Ho	0.72	0.73	102.0
<sup>166</sup> Er	2.18	2.09	95.9
<sup>169</sup> Tm	0.31	0.31	100.2
<sup>172</sup> Yb	2.1	2.00	95.1
<sup>175</sup> Lu	0.32	0.32	99.6
<sup>178</sup> Hf	3.48	3.45	99.1
<sup>181</sup> Ta	1.6	1.6	100.4
<sup>232</sup> Th	8.8	8.9	101.3
<sup>238</sup> U	1.6	1.6	99.1

## Appendix B.

Mantle and contaminant compositions (Table B1 and Fig. B1):

Modal mineralogy (Table B2):

**Modelling equations:**

Non-batch partial melting:

$$C_L = \frac{C_0}{D + F - FP} \quad (B.1)$$

Assimilation with concomitant fractional crystallisation:

$$C_L = C_0 \left( f' + \frac{r}{r - 1 + D} \cdot \frac{C_A}{C_0} (1 - f') \right) \quad (B.2)$$

$$f' = F^{-(r-1+D)/(r-1)} \quad (B.3)$$

Binary mixing (between magma and crustal assimilant):

$$C_{Mix} = \frac{C_{magma} + xC_A}{1 - x} \quad (B.4)$$

Fractional (Rayleigh) crystallisation:

$$C_L = C_0 F^{(D-1)} \quad (B.5)$$

$C_L$  = Concentration in liquid

$C_0$  = Initial concentration

$F$  = Fraction of melting

$D$  = Bulk distribution coefficient

$P$  = Bulk distribution coefficient of the minerals making up the melt

$C_{Mix}$  = Trace element concentration in resultant mixture

$C_{magma}$  = Concentration in uncontaminated magma

$C_A$  = Concentration in assimilant (e.g. contaminant)

$r$  = Ratio of assimilation rate to fractional crystallisation rate

$x$  = Fraction of assimilant added to the magma

**Partition coefficients (Table B3):**

Further ratio plots for trace element modelling (Fig. B2):

Mobility of PGE (Fig. B3):

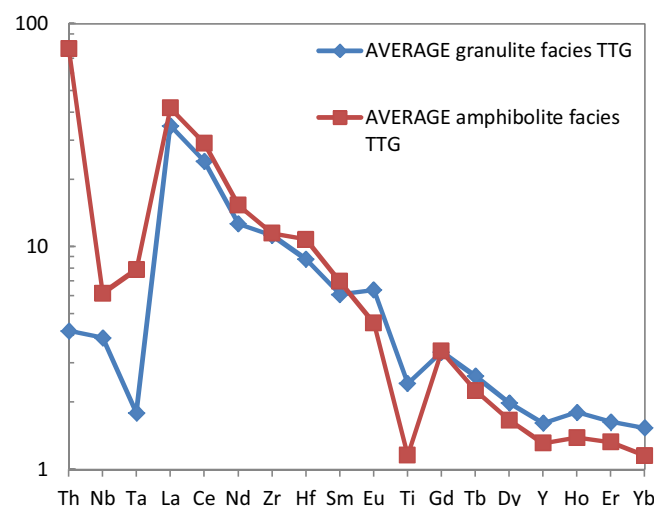


**Fig. B1.** Primitive mantle normalised multi-element plots for potential contaminants – Lewisian amphibolite and granulite, and Archaean SCLM partial melt. Average TTG compositions from Rollinson (2012).

**Table B1**

Trace element compositions of end members used in this study.

Element (ppm)	DMM <sup>a</sup>	EM1 <sup>b</sup>	PM <sup>c</sup>	Lewisian amphibolite <sup>d</sup>	Lewisian granulite TTG <sup>d</sup>
Th	0.01	0.03	0.08	6.14	0.33
Nb	0.15	0.38	0.66	4.06	2.57
Ta	0.01	0.03	0.04	0.29	0.07
La	0.19	0.60	0.65	27.1	22.6
Ce	0.55	1.75	1.68	48.7	40.5
Nd	0.58	1.47	1.25	19.1	15.8
Zr	5	13	10.5	121	118
Hf	0.16	0.36	0.28	3.04	2.48
Sm	0.24	0.52	0.41	2.83	2.48
Eu	0.10	0.20	0.15	0.70	0.98
Ti	716	1433	1205	1393	2930
Gd	0.36	0.72	0.54	1.84	1.83
Tb	0.07	0.13	0.10	0.22	0.26
Dy	0.51	0.92	0.67	1.12	1.34
Y	3.33	5.77	4.30	5.63	6.94
Ho	0.12	0.20	0.15	0.21	0.27
Er	0.35	0.60	0.44	0.58	0.72
Yb	0.37	0.62	0.44	0.51	0.68

<sup>a</sup> Workman and Hart (2005).<sup>b</sup> Willbold and Stracke (2006).<sup>c</sup> McDonough and Sun (1995).<sup>d</sup> Rollinson (2012).**Table B2**

Modal mineralogy spinel lherzolite, garnet lherzolite, transitional spinel-garnet lherzolite and partial melts.

	Olivine	Orthopyroxene	Clinopyroxene	Garnet	Spinel
Spinel lherzolite	0.55	0.25	0.18	0.00	0.02
Garnet lherzolite	0.55	0.20	0.15	0.10	0.00

Partial melts model mineralogy from Johnson et al. (1990).

**Table B3**

Partition coefficients used in geochemical modelling. Partition coefficient data from the following sources: Olivine – (Kelemen et al., 1993; Beattie, 1994; Bedini & Bodinier, 1999); Orthopyroxene – (McKenzie & O’Nions, 1991; Kelemen et al., 1993; Salters & Longhi, 1999); Clinopyroxene – (Hauri et al., 1994; Johnson, 1998); Spinel – (Kelemen et al., 1993; Elkins et al., 2008); Plagioclase – (Aigner-Torres et al., 2007); Magnetite – (Haskin et al., 1966; Okamoto, 1979; Lemarchand et al., 1987; Nielsen et al., 1992). Partition coefficients for Pr, Dy, Er, and Tm into magnetite are inferred. Ta coefficients have generally been inferred to be the same as Nb, unless published data is available. Partition coefficients for Pr, Gd, Tb, Ho, Tm, and Lu in silicates and spinel have been inferred where absent in the literature.

	Olivine	Orthopyroxene	Clinopyroxene	Spinel	Plagioclase	Magnetite
Th	0.0000001	0.0004	0.014	0.013	0.3435	0.1
Nb	0.0001	0.002825	0.00605	0.01	0.09725	0.7
Ta	0.0001	0.002825	0.00605	0.01	0.0795	0.23
La	0.000007	0.0000535	0.05025	0.0006	0.0631	0.015
Ce	0.00001	0.0026	0.089	0.0006	0.0457	0.016
Nd	0.00007	0.010267	0.178	0.0006	0.0478	0.026
Sm	0.0007	0.018	0.3775	0.0006	0.06575	0.024
Zr	0.0005	0.01775	0.1975	0.07	0.0094	0.71
Hf	0.0038	0.027225	0.2115	0.003	0.082	0.16
Eu	0.00095	0.0215	0.458	0.0006	0.3254	0.025
Ti	0.015	0.082	0.3955	0.15	0.0473	16.5
Gd	0.002	0.028	0.487	0.0009	0.07175	0.018
Tb	0.003	0.035	0.516	0.0012	0.084	0.019
Dy	0.004	0.041	0.5455	0.0015	0.057167	0.018
Y	0.007365	0.0935	0.412	0.002	0.00989	0.0039
Ho	0.0065	0.05	0.603	0.0023	0.0592	0.017
Er	0.009	0.063917	0.66	0.003	0.07633	0.017
Yb	0.023	0.093917	0.5165	0.0045	0.0903	0.018

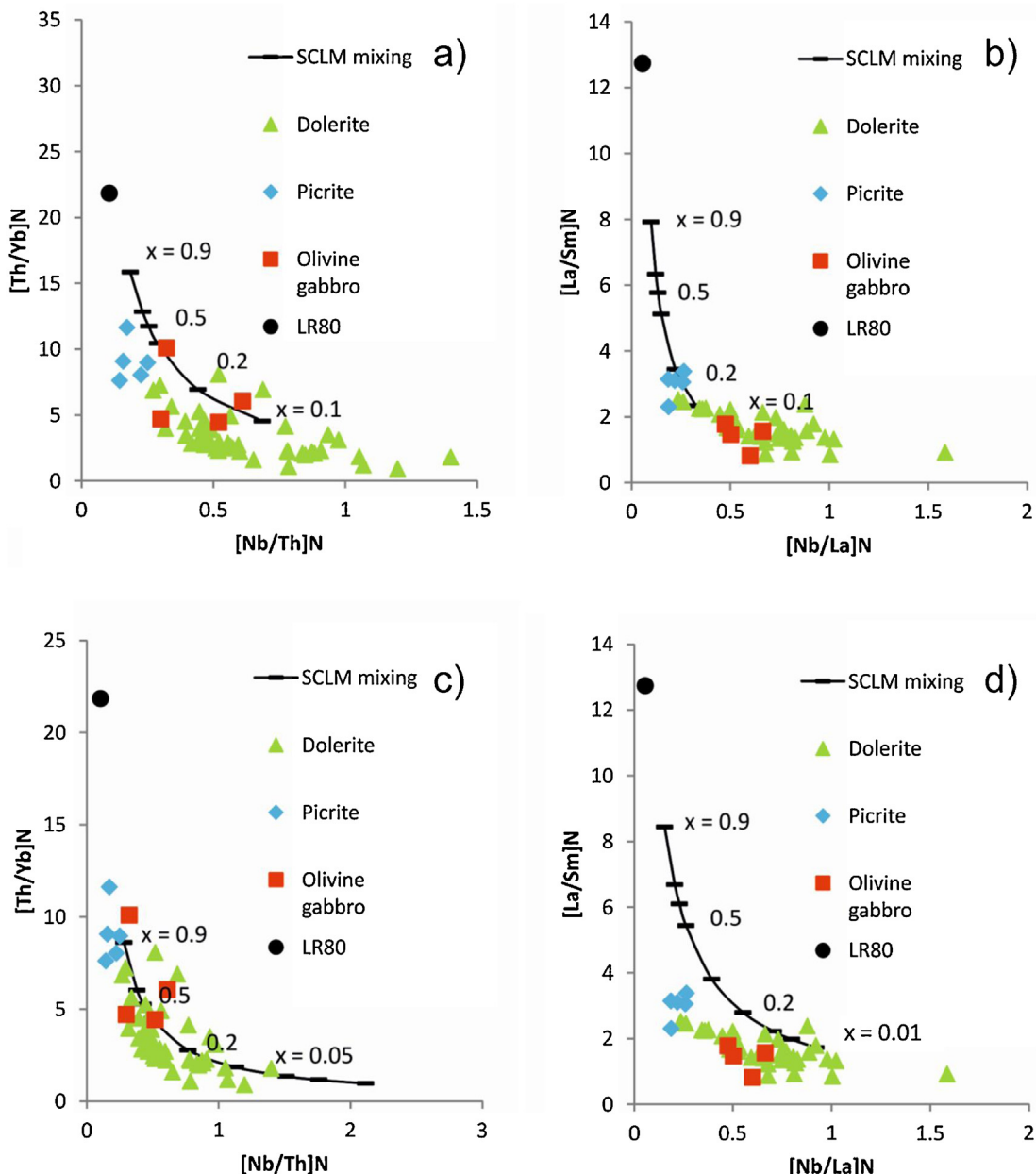


**Fig. B2.** Additional ratio plots (N denotes primitive mantle normalised ratios) for models described in Fig. 8 (main text). X is the fraction of SCLM partial melt mixed into model. No subsequent fractional crystallisation or AFC has been modelled in these plots, however assimilation of any Lewisian TTG partial melts would adjust La/Sm and Zr/Hf ratio (not plotted – see main text for discussion). (a) and (b) display model for picrite dykes – 10% partial melting of DMM garnet lherzolite mixing with 30% SCLM partial melt (LR80) in binary mixing model. (c) and (d) display model for dolerite dykes – 2–5% DMM spinel lherzolite partial melt mixing with 15% SCLM partial melt (LR80) in binary mixing model.

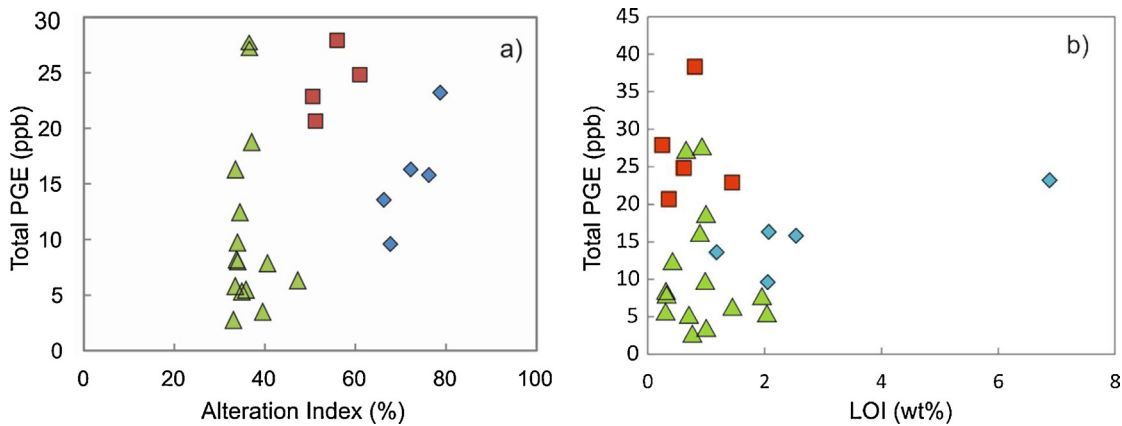


**Fig. B3.** PGE treated as immobile in Scourie Dykes – no correlation between PGE abundance (total) and any alteration index (as in plots (a) and (b). (a) Alteration Index (AI)=(K<sub>2</sub>O+MgO)/(Na<sub>2</sub>O+K<sub>2</sub>O+CaO+MgO)% used to assess PGE immobility during metamorphism and alteration. (b) Loss on ignition (LOI).

## Appendix C.

Os isotope systematics and model ages:

$^{187}\text{Os}/^{188}\text{Os}$  initial ( $\text{Os}_i$ )

$$\frac{^{187}\text{Os}}{^{188}\text{Os}_{\text{initial sample}}} = \left( \frac{^{187}\text{Os}}{^{188}\text{Os}_{\text{measured}}} - \frac{^{187}\text{Re}}{^{188}\text{Os}_{\text{measured}}} \right) \times (e^{[\lambda t]} - 1) \quad (1)$$

$\gamma\text{Os}$  (initial)

$$\gamma\text{Os}_i = \left( \left( \frac{^{187}\text{Os}}{^{188}\text{Os}_{\text{initial sample}}} \right) - 1 \right) \times 100 \quad (2)$$

$T_{\text{MA}}$  Os model ages, using  $\lambda$  ( $^{187}\text{Re}$  decay constant) of  $1.666 \times 10^{-11}$  (Lindner et al., 1989).

$$\text{Os}T_{\text{MA}} = \frac{1}{\lambda} \ln \left( \frac{\frac{^{187}\text{Os}}{^{188}\text{Os}_{\text{sample}}} - \frac{^{187}\text{Os}}{^{188}\text{Os}_{\text{O-chondrite}}}}{\frac{^{187}\text{Re}}{^{188}\text{Os}_{\text{sample}}} - \frac{^{187}\text{Re}}{^{188}\text{Os}_{\text{O-chondrite}}}} + 1 \right) \quad (3)$$

Re-depletion Os model age ( $T_{\text{RD}}$ ), which assumes all Re is metasomatic, so that model age is calculated so that  $\text{Re/Os} = 0$ .

$$\text{Os}T_{\text{RD}} = \frac{1}{\lambda} \ln \left( \frac{^{187}\text{Os}}{^{188}\text{Os}_{\text{sample}}} - \frac{^{187}\text{Os}}{^{188}\text{Os}_{\text{O-chondrite}}} + 1 \right) \quad (4)$$

Re-depletion model eruption age ( $T_{\text{RD}}^{\text{erupt}}$ ), which assumes all Re is metasomatic, but is calculated prior to time of magmatic sampling (i.e.,  $\text{Re/Os} = 0$ ) and  $\text{Re/Os}$  (measured) is corrected for radiogenic Os produced post-eruption. This expresses Os-isotopic composition at the time of eruption.

$$\text{Os}T_{\text{RD}}^{\text{erupt}} = \frac{1}{\lambda} \ln \left( \frac{^{187}\text{Os}}{^{188}\text{Os}_{\text{initial sample}}} - \frac{^{187}\text{Os}}{^{188}\text{Os}_{\text{initial O-chondrite}}} + 1 \right) \quad (5)$$

## Appendix References

Aigner-Torres, M., Blundy, J., Ulmer, P., Pettke, T., 2007. Laser ablation ICP-mS study of trace element partitioning between plagioclase and basaltic melts: an experimental approach. *Contributions to Mineralogy and Petrology*, 153, 647–667.

Beattie, P., 1994. Systematics and energetics of trace-element partitioning between olivine and silicate melts: implications for the nature of mineral/melt partitioning. *Chemical Geology*, 117, 57–71.

Bedini, R.M., Bodinier, J.L., 1999. Distribution of incompatible trace elements between the constituents of spinel peridotite xenoliths: ICP-MS data from the East African Rift. *Geochimica et Cosmochimica Acta*, 63, 3883–3900.

Elkins, L., Gaetani, G.A., Sims, K., 2008. Partitioning of U and Th during garnet pyroxenite partial melting: constraints on the source of alkaline ocean island basalts. *Earth and Planetary Science Letters*, 265, 270–286.

Haskin, L.A., Frey, F.A., Schmitt, R.A., Smith, R.H., 1966. Meteoric, solar and terrestrial rare-earth distributions. *Physical and Chemical Earth*, 7, 167–321.

Hauri, E.H., Wagner, T.P., Grove, T.L., 1994. Experimental and natural partitioning of Th, U, Pb and other trace elements between garnet, clinopyroxene and basaltic melts. *Chemical Geology*, 117, 149–166.

Johnson, K.T.M., 1998. Experimental determination of partition coefficients for rare earth and high-field-strength elements between clinoptyroxene, garnet, and basaltic melt at high pressures. *Contributions to Mineralogy and Petrology*, 133, 60–68.

Johnson, K.T.M., Dick, H.J.B., Shimizu, N., 1990. Melting in the Oceanic Upper Mantle: an ion microprobe study of diopsides in abyssal peridotites. *Journal of Geophysical Research*, 95, 2661–2678.

Kelemen, P.B., Shimizu, N., Dunn, T., 1993. Relative depletion of niobium in some arc magmas and the continental crust: partitioning of K, Nb, La and Ce during melt/rock reaction in the upper mantle. *Earth and Planetary Science Letters*, 120, 111–134.

Lemarchand, F., Benoit, V., Calais, G., 1987. Trace element distribution coefficients in alkaline series. *Geochimica et Cosmochimica Acta*, 51, 1071–1081.

Lindner, M., Leich, D.A., Russ, G.P., Bazan, J.M., Borg, R.J., 1989. Direct detection of the half-life of  $^{187}\text{Re}$ . *Geochimica et Cosmochimica Acta*, 53, 1597–1606.

McDonough, W.F. & Sun, S., 1995. The Composition of the Earth. *Chemical Geology*, 120, 223–253.

McKenzie, D., O’Nions, R.K., 1991. Partial melt distributions from inversion of rare earth element concentrations. *Journal of Petrology*, 32, 1021–1091.

Nielsen, R.L., Gallahan, W.E., Newberger, F., 1992. Experimentally determined mineral-melt partition coefficients for Sc, Y and REE for olivine, orthopyroxene, pigeonite, magnetite and ilmenite. *Contributions to Mineralogy and Petrology*, 110, 488–499.

Okamoto, K., 1979. Geochemical study on magmatic differentiation of Asama Volcano, central Japan. *Journal of Geological Society of Japan*, 85, 525–535.

- Rollinson, H., 2012. Geochemical constraints on the composition of Archaean lower continental crust: Partial melting in the Lewisian granulites. *Earth and Planetary Science Letters*, 351–352, 1–12.
- Salter, V.J.M., Longhi, J., 1999. Trace element partitioning during the initial stages of melting beneath mid-ocean ridges. *Earth and Planetary Science Letters*, 166, 15–30.
- Willbold, M., Stracke, A., 2006. Trace element composition of mantle end-members: Implications for recycling of oceanic and upper and lower continental crust. *Geochemistry Geophysics Geosystems*, 7.
- Workman, R.K., Hart, S.R., 2005. Major and trace element composition of the depleted MORB mantle (DMM). *Earth and Planetary Science Letters*, 231, 53–72.
- ## References
- Ahmed, A.H., Arai, S., 2002. Unexpectedly high-PGE chromitite from the deeper mantle section of the northern Oman ophiolite and its tectonic implications. *Contrib. Mineral. Petro.* 143, 263–278.
- Barnes, S.J., 1990. The use of metal ratios in prospecting for platinum-group element deposits in mafic and ultramafic intrusions. In: Dunn, C.E., Curtin, G.C., Hall, G.E.M. (Eds.), *Journal of Geochemical Exploration*, pp. 91–99.
- Barnes, S.J., Boyd, R., Korneliusen, A., Nilsson, L.P., et al., 1988. The use of mantle normalization and metal ratios in discriminating between the effects of partial melting, crystal fractionation and sulphide segregation on platinum group elements, gold, nickel and copper: examples from Norway. In: Prichard, H.M., Potts, P.J., Bowles, J.F.W., Cribb, S.J. (Eds.), *Geo Platinum*. Elsevier, London, pp. 113–143.
- Begg, G.C., Hronsky, J.A.M., Arndt, N.T., Griffin, W.L., et al., 2010. Lithospheric, cratonic, and geodynamic setting of Ni-Cu-PGE sulfide deposits. *Econ. Geol.* 105, 1057–1070.
- Bernstein, S., Kelemen, P.B., Brooks, C.K., 1998. Depleted spinel harzburgite xenoliths in Tertiary dykes from East Greenland: restites from high degree melting. *Earth Planet. Sci. Lett.* 154, 221–235.
- Bizzarro, M., Stevenson, R.K., 2003. Major element composition of the lithospheric mantle under the North Atlantic craton: evidence from peridotite xenoliths of the Sarfartoq area, southwestern Greenland. *Contrib. Mineral. Petro.* 146, 223–240.
- Bockrath, C., Ballhaus, C., Holzheid, A., 2004a. Fractionation of the platinum-group elements during mantle melting. *Science* 305, 1951–1953.
- Bockrath, C., Ballhaus, C., Holzheid, A., 2004b. Stabilities of laurite Ru<sub>2</sub>S and monosulphide solid solution at magmatic temperatures. *Chem. Geol.* 208, 265–271.
- Brenan, J.M., Andrews, D., 2001. High-temperature stability of laurite and Ru-Os-Ir alloy and their role in PGE fractionation in mafic magmas. *Can. Mineral.* 39, 341–360.
- Bridgwater, D., Mengel, F., Fryer, B., Wagner, P., et al., Special Publications 95 1995. Early Proterozoic mafic dykes in the North Atlantic and Baltic cratons: field setting and chemistry of distinctive dyke swarms. Geological Society, London, pp. 193–210.
- Buchan, K.L., Mertanen, S., Park, R.G., Pensonen, L.J., et al., 2000. Comparing the drift of Laurentia and Baltica in the Proterozoic: the importance of key palaeomagnetic poles. *Tectonophysics* 319, 167–198.
- Cartwright, I., Valley, J.W., 1991. Low-<sup>18</sup>O Scourie dyke magmas from the Lewisian complex, northwestern Scotland. *Geology* 19, 578–581.
- Crocket, J.H., 2000. PGE in fresh basalt, hydrothermal alteration products, and volcanic incrustations of Kilauea volcano, Hawaii. *Geochim. Cosmochim. Acta* 64, 1791–1807.
- Davies, G.F., 2009. Effect of plate bending on the Urey ratio and the thermal evolution of the mantle. *Earth Planet. Sci. Lett.* 287, 513–518.
- Davies, J.H.F.L., Heaman, L.M., 2014. New U-Pb baddeleyite and zircon ages for the Scourie dyke swarm: a long-lived large igneous province with implications for the Paleoproterozoic evolution of NW Scotland. *Precambrian Res.*
- Davies, J.H.F.L., Heaman, L.M., DuFrane, S.A., Muehlenbachs, K., et al., 2012. *Geochemical and Isotopic Insights into the Origin of the 'Scourie' Dykes*. Goldschmidt, Montreal.
- Ernst, R.E., Bleeker, W., Söderlund, U., Kerr, A.C., 2013. Large Igneous Provinces and supercontinents: toward completing the plate tectonic revolution. *Lithos* 174, 1–14.
- Faithfull, J.W., Timmerman, M.J., Upton, B.G.J., Rumsey, M.S., 2012. Mid-Eocene renewal of magmatism in NW Scotland: the Loch Roag Dyke, Outer Hebrides. *J. Geol. Soc.* 169, 115–118.
- Fettes, D.J., Mendum, J.R., Special Publications 27 1987. *The Evolution of the Lewisian Complex in the Outer Hebrides*. Geological Society, London, pp. 27–44.
- Fowler, M.B., 1986. Large-ion lithophile element characteristics of an amphibolite facies to granulite facies transition at Gruinard Bay, North-west Scotland. *J. Metamorph. Geol.* 4, 345–359.
- Frick, L.R., PhD 1998. Application of Re-Os isotopes to the study of lithospheric processes in Archaean terrains. Monash University.
- Frick, L.R., Lambert, D.D., Reeves, S.J., Heaman, L.M., 1994. Platinum-group element and osmium isotope evidence for the origin of Scourie Dykes. *Goldschmidt 1994 Edinburgh. Mineral. Magaz.*, 290–291.
- Friend, C.R.L., Kinny, P.D., 2001. A reappraisal of the Lewisian Gneiss Complex: geochronological evidence for its tectonic assembly from disparate terranes in the Proterozoic. *Contrib. Mineral. Petro.* 142, 198–218.
- Gallagher, K., Hawkesworth, C.J., 1992. Dehydration melting and the generation of continental flood basalts. *Nature* 358, 57–59.
- Gammoms, C.H., Bloom, M.S., 1993. Experimental investigation of the hydrothermal geochemistry of platinum and palladium: II. The solubility of PtS and PdS in aqueous sulfide solutions to 300 °C. *Geochim. Cosmochim. Acta* 57, 2451–2467.
- Goodenough, K.M., Crowley, Q.G., Krabbendam, M., Parry, S.F., 2013. New U-Pb age constraints for the Laxford Shear Zone NW Scotland: evidence for tectono-magmatic processes associated with the formation of a Paleoproterozoic supercontinent. *Precambrian Res.* 233, 1–19.
- Goodenough, K.M., Park, R.G., Krabbendam, M.K., Myers, J.S., et al., 2010. The Laxford Shear Zone: an end-Archaean terrane boundary? In: Law, R.D., Butler, R.W.H., Holdsworth, R.E., Krabbendam, M. (Eds.), *Continental Tectonics and Mountain Building. The Legacy of Peach and Horne*. The Geological Society of London, London, pp. 103–120, Special Publication No. 335.
- Griffin, W.L., O'Reilly, S.Y., Afonso, J.C., Begg, G.C., 2008. The composition and evolution of lithospheric mantle: a re-evaluation and its tectonic implications. *J. Petrol.* 50, 1185–1204.
- Griffin, W.L., O'Reilly, S.Y., Abe, N., Aulbach, S., et al., 2003. The origin and evolution of Archaean lithospheric mantle. *Precambrian Res.* 127, 19–41.
- Hanghoj, K., Kelemen, P.B., Bernstein, S., Blusztajn, J., et al., 2001. Osmium isotopes in the Wiedemann Fjord mantle xenoliths: a unique record of cratonic mantle formation by melt depletion in the Archaean. *Geochem. Geophys. Geosyst.* 2, 1–14.
- Hawkesworth, C.J., Gallagher, K., Hergt, J.M., McDermott, F., 1994. Destructive plate margin magmatism: geochemistry and melt generation. *Lithos* 33, 169–188.
- Heaman, L.M., Tarney, J., 1989. U-Pb baddeleyite ages for the Scourie Dyke Swarm, Scotland: evidence for two distinct intrusion events. *Nature* 340, 705–708.
- Herzberg, C., Condé, K., Korenaga, J., 2010. Thermal history of the Earth and its petrological expression. *Earth Planet. Sci. Lett.* 292, 79–88.
- Hofmann, A.W., 1997. Mantle geochemistry: the message from oceanic volcanism. *Nature* 385, 219–229.
- Holland, J.G., Lambert, R.S.J., 1973. Comparative major element geochemistry of the Lewisian of the mainland of Scotland. In: Park, R.G., Tarney, J. (Eds.), *The Early Precambrian of Scotland and related rocks of Greenland*. University of Keele, Keele, pp. 51–62.
- Huber, H., Koeberl, C., McDonald, I., Reimond, W.U., 2000. Use of  $\gamma$ - $\gamma$  coincidence spectrometry in the geochemical study of diamictites from South Africa. *J. Radioanal. Nucl. Chem.* 244, 603–607.
- Ionov, D.A., Harmer, R.E., 2002. Trace element distribution in calcite-dolomite carbonates from Spitskop: Inferences for differentiation of carbonate magmas and the origin of carbonates in mantle xenoliths. *Earth Planet. Sci. Lett.* 198, 495–510.
- Ishikawa, Y., Sawaguchi, T., Iwaya, S., Horiuchi, M., 1976. Delineation of prospecting targets for Kuroko deposits based on modes of volcanism of underlying dacite and alteration halos. *Mining Geol.* 26, 105–117.
- Jenner, F.E., Bennett, V.C., Yaxley, G., Friend, C.R.L., et al., 2013. Eoarchean within-plate basalts from southwest Greenland. *Geology* 41, 327–330.
- Jenner, G.A., 1996. Trace element geochemistry of igneous rocks: geochemical nomenclature and analytical geochemistry. In: Wyman, D.A. (Ed.), *Trace Element Geochemistry of Volcanic Rocks: Applications for Massive Sulphide Exploration*. Geological Association of Canada, Winnipeg, pp. 51–78.
- Johnstone, G.S., Mykura, W., 1989. Lewisian. In: British Regional Geology: The Northern Highlands of Scotland. British Geological Survey, Nottingham, pp. 13–29.
- Kalsbeek, F., Bridgwater, D., Zeck, H., 1987. A 1950+60 Ma Rb-Sr isochron age from two Kangamiut dykes and the timing of the Nagssugtoqidian (Hudsonian) orogeny in West Greenland. *Can. J. Earth Sci.* 15, 1122–1128.
- Keays, R.R., 1982. Palladium and iridium in komatiites and associated rocks: application to petrogenetic problems. In: Arndt, N.T., Nisbet, E.G. (Eds.), *Komatiites*. George Allen and Unwin, London, pp. 435–455.
- Keays, R.R., 1995. The role of komatiitic and picritic magmatism and S-saturation in the formation of ore deposits. *Lithos* 34, 1–18.
- Kinny, P.D., Friend, C.R.L., Love, G.J., 2005. Proposal for a terrane-based nomenclature for the Lewisian Gneiss Complex of NW Scotland. *J. Geol. Soc.* 162, 175–186.
- Korenaga, J., 2008. Urey ratio and the structure and evolution of the Earth's mantle. *Rev. Geophys.* 46, 1–32.
- Le Maître, R.W., Streckenbach, A., Zanettin, B., Le Bas, M.J., et al., 2002. *Igneous Rocks: A Classification and Glossary of Terms*, Recommendations of the International Union of Geological Sciences. Cambridge University Press, Cambridge, UK.
- Long, A.M., Menzies, M.A., Thirlwall, M.F., Upton, B.G.J., et al., 1991. Carbonatite-mantle interaction: a possible origin for megacryst/xenolith suites in Scotland. In: Meyer, H.O.A., Leonards, O.H. (Eds.), *Fifth International Kimberlite Conference*, Brazil.
- Love, G.J., Friend, C.R.L., Kinny, P.D., 2010. Palaeoproterozoic terrane assembly in the Lewisian Gneiss Complex on the Scottish mainland, south of Gruinard Bay: SHRIMP U-Pb zircon evidence. *Precambrian Res.* 183, 89–111.
- Love, G.J., Kinny, P.D., Friend, C.R.L., 2003. Timing of magmatism and metamorphism in the Gruinard Bay area of the Lewisian Gneiss Complex: comparisons with the Assynt Terrane and implications for terrane accretion. *Contrib. Mineral. Petro.* 146, 620–636.

- Maier, W.D., Barnes, S.-J., 2004. Pt/Pd and Pd/Ir ratios in mantle-derived magmas: a possible role for mantle metasomatism. *S. Afr. J. Geol.* 107, 333–340.
- Martin, H., Moyen, J.-F., Rapp, R., 2010. The sanukitoid series: magmatism at the Archaean-Proterozoic transition. *Geol. Soc. Am. Spec. Pap.* 472, 15–33.
- Mason, A.J., Brewer, T.S., 2004. Mafic dyke remnants in the Lewisian Complex of the Outer Hebrides, NW Scotland: a geochemical record of continental break-up and re-assembly. *Precambrian Res.* 133, 121–141.
- McDonald, I., De Wit, M., Smith, C.B., Bizzi, L.A., et al., 1995. The geochemistry of the platinum-group elements in Brazilian and southern African kimberlites. *Geochim. Cosmochim. Acta* 59, 2883–2903.
- McDonald, I., Viljoen, K.S., 2006. Platinum-group element geochemistry of mantle eclogites: a reconnaissance study of xenoliths from the Orapa kimberlite, Botswana. *Applied Earth Science* 115, 81–93.
- McDonough, W.F., Sun, S., 1995. The Composition of the Earth. *Chem. Geol.* 120, 223–253.
- McKenzie, D., Bickle, M.J., 1988. The volume and composition of melt generated by extension of the lithosphere. *J. Petrol.* 29, 625–679.
- Menzies, M.A., Halliday, A.N., Palacz, Z., Hunter, R.N., et al., 1987. Evidence from mantle xenoliths for an enriched lithospheric keel under the Outer Hebrides. *Nature* 325, 44–47.
- Muir, R.J., Evans, J.A., Fitches, W.R., 1993. Mafic dykes within the Lewisian Complex on Tiree and Coll, Inner Hebrides. *Scott. J. Geol.* 29, 167–176.
- Naldrett, A.J., 2011. Fundamentals of magmatic sulfide deposits. In: Li, C., Ripley, E.M. (Eds.), *Magmatic Ni-Cu and PGE Deposits: Geology, Geochemistry, and Genesis*. Society of Economic Geologists, Reviews in Economic Geology, vol. 17, pp. 1–51.
- Nilsson, M.K.M., Klausen, M.B., Söderlund, U., Ernst, R.E., 2013. Precise U–Pb ages and geochemistry of Palaeoproterozoic mafic dykes from southern West Greenland: linking the North Atlantic and the Dharwar cratons. *Lithos* 174, 255–270.
- O'Hara, M.J., 1961. Petrology of the Scourie dykes, Sutherland. *Mineral. Magaz.* 32, 848–865.
- O'Reilly, S.Y., Griffin, W.L., Poudjom Djomani, Y.H., Morgan, P.O., 2001. Are lithospheres forever? Tracking changes in subcontinental lithospheric mantle through time. *GSA Today*, 4–10.
- Park, R.G., 1994. Early Proterozoic tectonic overview of the northern British Isles and neighbouring terrains in Laurentia and Baltica. *Precambrian Res.* 68, 65–79.
- Park, R.G., 1995. Palaeoproterozoic Laurentia–Baltica relationships: a view from the Lewisian. In: Coward, M.P., Ries, A.C. (Eds.), *Early Precambrian Processes*. The Geological Society, London, Geological Society Special Publication 95.
- Park, R.G., 2002. The Scourie Dyke Suite. Geological Society Memoirs, 26. The Geological Society, London, pp. 21–28.
- Park, R.G., Kinny, P.D., Friend, C.R.L., Love, G.J., 2005. Discussion on a terrane-based nomenclature for the Lewisian Gneiss Complex of NW Scotland. *J. Geol. Soc. (London)* 162, 893–895.
- Park, R.G., Tarney, J., 1987. The Lewisian complex: a typical Precambrian high-grade terrain? In: Park, R.G., Tarney, J. (Eds.), *Evolution of the Lewisian and Comparable Precambrian High Grade Terrains*. The Geological Society, pp. 13–25.
- Peach, B.N., Horne, J., Gunn, W., Clough, C.T., et al., 1907. *The Geological Structure of the North-West Highlands of Scotland*. Her Majesty's Stationery Office, London.
- Pearce, J.A., 1996. A user's guide to basalt discrimination diagrams. In: Wyman, D.A. (Ed.), *Trace Element Geochemistry of Volcanic Rocks: Applications for Massive Sulphide Exploration*. Geological Association of Canada, Winnipeg, pp. 79–114.
- Pearce, J.A., 2008. Geochemical fingerprinting of oceanic basalts with applications to ophiolite classification and the search for Archean oceanic crust. *Lithos* 100, 14–48.
- Pearce, J.A., Stern, R.J., Bloomer, S.H., Fryer, P., 2005. Geochemical mapping of the Mariana arc-basin system: implications for the nature and distribution of subduction components. *Geochem. Geophys. Geosyst.* 6.
- Pearson, D.G., Canil, D., Shirey, S.B., 2003. Mantle samples included in volcanic rocks: Xenoliths and diamonds. In: *Treatise on Geochemistry*, pp. 171–275.
- Polat, A., Kerrich, R., 2006. Reading the geochemical fingerprints of Archean hot subduction volcanic rocks: Evidence for accretion and crustal recycling in a mobile tectonic regime. *Am. Geophys. Union: Geophys. Monogr. Ser.* 164, 189–213.
- Richter, F.M., 1988. A major change in the thermal state of the earth at the Archean-Proterozoic Boundary: consequences for the nature and preservation of continental lithosphere. *J. Petrol.* 29, 39–52.
- Rollinson, H., 2010. Coupled evolution of Archean continental crust and subcontinental lithospheric mantle. *Geology* 38, 1083–1086.
- Rollinson, H., 2012. Geochemical constraints on the composition of Archean lower continental crust: partial melting in the Lewisian granulites. *Earth Planet. Sci. Lett.* 351–352, 1–12.
- Rollinson, H.R., Fowler, M.B., 1987. The magmatic evolution of the Scourian complex at Gruinard Bay. In: Park, R.G., Tarney, J. (Eds.), *Evolution of the Lewisian and comparable Precambrian High Grade Terrains*. Geological Society of London, pp. 57–71, Special Publication No. 27.
- Rudnick, L., Fountain, D.M., 1995. Nature and composition of the continental crust: a lower crustal perspective. *Rev. Geophys.* 33, 267–309.
- Sand, K.K., Waught, T.E., Pearson, D.G., Nielsen, T.F.D., 2009. The lithospheric mantle below southern West Greenland: a geothermobarometric approach to diamond potential and mantle stratigraphy. *Lithos* 112, 1155–1166.
- Sattari, P., Brenan, J.M., Horn, I., McDonough, W.F., 2002. Experimental constraints on the sulfide- and chromite-silicate melt partitioning behavior of rhenium and the platinum-group elements. *Econ. Geol.* 97, 385–398.
- Selby, D., Kelley, K.D., Hitzman, M.W., Zieg, J., 2009. Re-Os sulphide (Bornite, Chalcocite, and Pyrite) systematic of the Carbonate-hosted copper deposits at Ruby Creek, Southern Brooks Range, Alaska. *Econ. Geol.* 104, 437–444.
- Sheraton, J.W., Skinner, A.C., Tarney, J., 1973. The geochemistry of the Scourian gneisses of the Assynt district. In: Park, R.G., Tarney, J. (Eds.), *The Early Precambrian of Scotland and Related Rocks of Greenland*. University of Keele, Keele, pp. 13–30.
- Sutton, J., Watson, J.V., 1951. The pre-Torridonian metamorphic history of the Loch Torridon and Scourie areas in the NW Highlands and its bearing on the chronological classification of the Lewisian. *J. Geol. Soc. (London)* 106, 241–308.
- Tappe, S., Smart, K.A., Pearson, D.G., Steenfelt, A., et al., 2011. Craton formation in Late Archean subduction zones revealed by first Greenland eclogites. *Geology* 39, 1103–1106.
- Tarney, J., 1963. Assynt dykes and their metamorphism. *Nature* 199, 672–674.
- Tarney, J., 1973. The Scourie dyke suite and the nature of the Inverian event in Assynt. In: Park, R.G., Tarney, J. (Eds.), *The Early Precambrian of Scotland and Related Rocks of Greenland*. University of Keele, Keele, pp. 105–118.
- Tarney, J., Weaver, B.L., 1987. Mineralogy, petrology and geochemistry of the Scourie dykes: petrogenesis and crystallization processes in dykes intruded at depth. In: Park, R.G., Tarney, J. (Eds.), *Evolution of the Lewisian and comparable Precambrian High Grade Terrains*. The Geological Society, pp. 217–234.
- Upton, B.G.J., Downes, H., Kirstein, L.A., Bonadiman, C., et al., 2011. The lithospheric mantle and lower crust-mantle relationships under Scotland: a xenolithic perspective. *J. Geol. Soc.* 168, 873–886.
- Upton, B.J.G., Aspen, P., Chapman, N.A., 1983. The upper mantle and deep crust beneath the British Isles: evidence from inclusions in volcanic rocks. *J. Geol. Soc. 140*, 105–121.
- van Gool, J.A.M., Connelly, J.N., Marker, M., Mengel, F.C., 2002. The Nagssugtoqidian Orogen of West Greenland: tectonic evolution and regional correlations from a West Greenland perspective. *Can. J. Earth Sci.* 39, 665–686.
- Waters, F.G., Cohen, A.S., O'Nions, R.K., O'Hara, M.J., 1990. Development of Archean lithosphere deduced from chronology and isotope chemistry of Scourie Dykes. *Earth Planet. Sci. Lett.* 97, 241–255.
- Vernon, R., Holdsworth, R.E., Selby, D., Dempsey, E., et al., 2014. Structural characteristics and Re-Os dating of quartz-pyrite veins in the Lewisian Gneiss Complex, NW Scotland: evidence of an Early Paleoproterozoic hydrothermal regime during terrane amalgamation. *Precambrian Res.* 1–37.
- Weaver, B.L., Tarney, J., 1981a. Chemical changes during dyke metamorphism in high-grade basement terrains. *Nature* 289, 47–49.
- Weaver, B.L., Tarney, J., 1981b. The Scourie Dyke Suite: petrogenesis and geochemical nature of the Proterozoic sub-continental mantle. *Contrib. Mineral. Petro.* 78, 175–188.
- Willbold, M., Stracke, A., 2006. Trace element composition of mantle end-members: implications for recycling of oceanic and upper and lower continental crust. *Geochem. Geophys. Geosyst.* 7.
- Wittig, N., Pearson, D.C., Webb, M., Ottley, C.J., et al., 2008. Origin of cratonic lithospheric mantle roots: a geochemical study of peridotites from the North Atlantic Craton, West Greenland. *Earth Planet. Sci. Lett.* 274, 24–33.
- Wittig, N., Webb, M., Pearson, D.G., Dale, C.W., et al., 2010. Formation of the North Atlantic Craton: timing and mechanisms constrained from Re-Os isotope and PGE data of peridotite xenoliths from S.W. Greenland. *Chem. Geol.* 276, 166–187.
- Workman, R.K., Hart, S.R., 2005. Major and trace element composition of the depleted MORB mantle (DMM). *Earth Planet. Sci. Lett.* 231, 53–72.
- Yaxley, G., Crawford, A.J., Green, D.H., 1991. Evidence for carbonatite metasomatism in spinel peridotite xenoliths from western Victoria, Australia. *Earth Planet. Sci. Lett.* 107, 305–317.
- Yaxley, G.M., Green, D.H., Kamenetsky, V., 1998. Carbonatite metasomatism in the southeastern Australian lithosphere. *J. Petrol.* 39, 1917–1930.
- Zhu, W., Zhang, Z., Shu, L., Lu, H., et al., 2008. SHRIMP U–Pb zircon geochronology of Neoproterozoic Korla mafic dykes in the Northern Tarim Block, NW China: Implications for the long-lasting breakup process of Rondinia. *J. Geol. Soc. (London)* 165, 887–890.